Motion and Total Force Distribution for a Floating Marine Structure in Finite-Depth Water

by
Jin S. Chung*

Abstract

A potential flow approach is used to develop a method and an associated computer program for floating marine structures of general configuration in waves of all water depths with arbitrary heading. It computes the total force distributions and six degrees-of-freedom motion. The hydrodynamic-force equations derived become identical under certain assumptions to the equations commonly used by the offshore industry, and the two methods are compared in detail. The computed motions of all six degrees agree quite well with model-scale and full-scale experimental data for two typical semisubmersible drilling rigs in finite-depth water. Also the present motion computations are more accurate than a previous work by the second approach. The present computations use experimentally validated or determined values of frequency-dependent hydrodynamic coefficients with the effects of the free surface and both finite and infinite water depths. The present method generates sufficient computation accuracy to use for practical design applications,

Nomenclature

A: incident wave amplitute (half the wave height)
A_{ci}: cross-sectional area of the i^{th} column segment
A_{hi}: cross-setional area of the i^{th} hull segment
A_{cwi}: waterplane area of the i^{th} column segment
A_{hwi}: waterplane area of the i^{th} hull segment
A_{wpi}: $A_{cwi}+A_{hwi}$
A_{jk}: added-mass coefficients (j, $k=1,2...6$)
B_{jk}: damping coefficients (j, $k=1$, 2...6)
C_{jk}: restoring force coefficients (j, $k=1$, 2...6)
C_d: viscous drag coefficient
C_x: crosssection of the i^{th} segment
D: viscous drag or damping force
E_1: wave energy
E_r: motion energy
F_j: exciting forces and moments ($j=1,2...6$)
H_i: wetted length of the i^{th} column segment
H_{ji}: linear viscous and wave damping forces for the i^{th} hull segment in the i^{th} mode ($j=1,2,3$)
$H_{1/3}$: significant wave height (average of the 1/3-highest wave heights)
I_j: rig moment of inertia in the j^{th} mode ($j=1,2,3$)
L_i: length of the i^{th} hull segment
M: rig mass
R_e: Reynolds number
R_r: transfer function
R_s: response motion energy spectrum density
$R_{1/3}$: significant motion in double amplitude
S_1: wave spectral energy density
S_{ci}: principal prefected area of the i^{th} column segment
S_{hi}: principal projected area of the i^{th} hull segment
T: wave period (sec)
V_i: volume of the i^{th} segment
V: rig volume
X_j: total force components on the rig in the j^{th} mode
X_j^{F-K}: Froude-Krilov force
X_j^D: diffraction force
X_j^M: motion-dependent force
a: radius or characteristic cross-sectional dimension

*Member

of cylindrical member

a_{jk}: segmental added-mass coefficients ($j,k=1,2,3$)

b: vertical distance of the rig C.G. above the mean free surface

b_{jk}: segmental damping coefficients ($j,k=1,2,3$)

c_{jk}: segmental hydrostatic restoring coefficients ($j,k=1,2...6$)

c: subscript to denote pertinence to column members

d_{ci}: diameter of the i^{th} column segment

d_{ki}: diameter of the i^{th} hull segment

dl_i: element of arc along the cross-section C_x of the i^{th} segment

dx_L: length variable along the length of the i^{th} segment

ds_i: $dx_L\ dl_i$

g: gravity acceleration

h: hulls as a subscript

h: water depth

k: wave number

k_1: $k \sin \beta_1$

k_2: $k \cos \beta_1$

m_{ci}: mass displaced by the i^{th} column segment

m_{hi}: mass displaced by the i^{th} hull segment

Δm_{cji}: $a_{jj}H_i$

Δm_{hji}: $a_{jj}L_i$

n_j: generalized normal ($j=1,2,3$)

s_i: surface of the i^{th} segment

t: time

v_j: water-particle oscillatory velocity for the j^{th} mode

$\dot{v}_j$: water-particle oscillatory acceleration for the j^{th} mode

v'_{ji}: relative velocity of the i^{th} segment for the j^{th} mode of motion

x_j: $x_i=x_1$, $y_i=x_2$, and $z_i=x_3$

x,y,z: Cartesian body coordinate system as defined in Fig. 2.

x_i, y_i, z_i: segment coordinate system as defined in Fig.2

z_ϕ: transverse metacentric height

z_θ: longitudinal metacentric height

z_{hi}: the vertical distance of the hull segment axis below the rig C.G.

α: angle of incoming wave direction relative to the (x,y,z) coordinate

β_i: angle of incoming wave direction relative to the (x_i,y_i,z_i)

γ_i: angle between the x-and x_i-axis

ϵ_j: phase angles for the j^{th} mode of motions ($j=1,2...6$)

ξ,η,ζ: rectilinear translatory displacements: surge, sway, and heave, respectively (x_j, $j=1,2,3$)

ξ_i,η_i,ζ_i: displacements of the i^{th} segment point in the x_i-, y_i-, and z_i-directions, respectively

ϕ,θ,Ψ: angular rotatory displacements: roll, pitch, and yaw, respectively (x_j, $j=4,5,6$)

Φ: velocity potential

ϕ_I: amplitude of the incident wave potential

ϕ_D: amplitude of the diffraction potential

ϕ_j: amplitude of the oscillatory potential

ρ: sea water density

ζ: wave-surface profile

T_i: $k_1x_{ci}-k_2y_{ci}-\omega t$

x_j: motion displacements in the j^{th} mode ($j=1,2...6$)

ω: wave frequency in rad/sec

$\bar{\omega}$: dimensionless frequency ($\bar{\omega}=\omega^2a/g$)

μ_{cji}, μ_{hji}: segmental (two dimensional) added-mass coefficient on the i^{th} column and hull segments, respectively for the j^{th} mode ($j=1,2,3$)

$\lambda_{cji}, \lambda_{hji}$: segmental (two dimensional) wave-damping coefficient on the i^{th} column and hull segments, respectively for the j^{th} mode ($j=1,2,3$)

λ: wavelength

1. Introduction

Two approaches in general have been used for the eqnations of the hydrodynamic forces for a floating structure in waves. The "first" approach is to derive the linear equations by a potential flow approach. The "second" approach commonly used in the offshore engineering applications is to directly use the equations of wave-induced inertia force and damping force: this approach has been more commonly used in the coastal engineering [7, 20]. The first approach was used by an investigator [8] for a floating platform problem in waves of infinite depth: his equations of motion are coupled between a pair of three modes of motion: surge-heave-pitch and sway-roll-yaw, the submerged members are parallel to each other, and the structure

has a lateral symmetry. The second approach was initially used by Bain [1, 10] and has been used by many other investigators [3, 4, 6, 11, 12]: the equations and computations in [10] are obtained by [1]; the equations used by the second approach share many major features and differ in some detail only;and the motion computations neglected the effects of the free surface and water depth on the hydrodynamic coefficients. [1, 4, 11, 12] show the motion computations for infinite water depth. [3] computed the six degrees of motion for both deep water and finite-depth water; the extent of the coupling between the modes of motion is not stated. [6] computed motions of vertical modes only. [3, 4, 6, 11] ignored without proper justification the coupling of the hydrodynamic coefficients for the member segments of arbitrary shapes. Also all these papers did not relate the results to the industrial practise.

The present equations of the linear hydrodynamic forces are derived with a potential flow approach similar to [14] used for the ship-motion problem, and are reduced with a few reasonable assumptions to the same equations as the equations used by the second approach. The total force is a sum of the linear forces; the wave or exciting force (sum of "Froude-Krilov" force and "diffraction" force), the hydrostatic force, and the "motion-dependent" force (due to the segment motion in still water). For the structure of general configuration, structural members can be arbitrarily arranged and nearly all modes of motion are coupled. All coupled motions of six degrees are computed for both finite and infinite water depths with the hydrodynamic coefficients including the effects of the free surface and water depth. The coupling of the hydrodynamic coefficients for the segments of arbitrary shape is described. The mathematical treatment and the result interpretation are related to the operational practices. Summary in the above describes more about the present method. Ultimate purpose of developing such method and computer program is in its application to the design for the safety and economy of the floating-rig construction and operations.

In design of floating structures such as semisubmersible drilling rigs, to have small rigs' motion amplitudes is required to conduct safe, economical, floating-drilling operations. Presently, the finite-depth offshore drilling is most active. The heave and other modes (roll, pitch, surge, sway, and yaw) of large motions can increase costly weather downtime. There are several weatherdowntime parameters which have an influence on the operational performance of the floating drilling rig, and the amount of time in which it can perform useful work. Included in these are the motion of the rig, anchor-holding conditions, station-keeping ability, and stressing and general performance of the marine riser. The experiences indicate that the floating-drilling operations may be shut down due to the excessive rig motion: limiting maximum heave in double amplitude is about 10 feet (3.048m), and limiting maximum roll and pitch in double amplitude are 4 degrees. Shutting down entails hanging the drill pipe at the seabed level, making the well safe and retrieving the marine riser. Several of many operations other than drilling which have to be conducted have small-amplitude motion limit, such as well logging, flow testing, running the "blow-out-preventor" (BOP) stack and running and pulling the marine riser. Also there is the lower operational limitations of the work-boat motions for the deployment and retrieval of the anchors and mooring lines. Structural analysis of the design needs the accurate total-force distribution along the structural members. The dynamic-tension computation of the mooring lines needs the motion of the point of the mooring-line top. To design a floating structure with minimum motion characteristic and the structural adequacy and reduce the need for expensive, time-consuming model tests, a method of accurately computing motions and total force distributions is a good engineering tool in the preliminary design. Since the present paper has its emphasis on the theoretical treatment as well as the pratical applications, the equations of the total forces and motion are formally derived in the first two sections. Discussions on the hydrodynamic coefficients of the tests of the method's validity follows with practical data, and a practical interpretation of the method is disussed.

2. Formulation of Equations of Motion

A majority of floating, multihull marine structures such as semisubmersible drilling rigs consists mainly

of tubular, cylindrical structural members of various cross-sectional shapes. These members are either submerged or semi-submerged. The geometry and arrangement of the submerged portion of the individual members differ from one design to another, causing different motions for given sea states.

The slopes of the incident waves are assumed to be small: the waves may be described as infinitesimal. The incident waves diffract upon the structural members and scatter in all directions and set the floating structure into motion, and the motion of the structural members generates additional waves in all diections. The floating structure or rig is assumed to undergo a linear rigid-body motion with six degrees-of-freedom motion in waves. The structural members are idealized as many continuous member segments consisting of (vertical) column segments and (horizontal) hull segments (Fig. 2). The hydrodynamic treatment of the structure is made on each individual segment, submerged or semi-submerged. Then these individual hydrodynamic quantities can properly be summed over the entire submerged portion of the structure.

A Cartesian body coordinate sxstem (x,y,z) has its origin at the center of gravity (CG) of a structure with the undisturbed free surface at (o, o, −b) (Fig. 2). The x-axis is positive forward, the y-axis is positive toward port, and the z-axis is positive upward. Additionally, a body coordinate system(x_i, y_i, z_i) is introduced with its origin at (x_{ci}, y_{ci}, 0) of the i^{th} segment. The x_i-*axis* is along the i^{th} hull-segment axis, and the z_i-*axis* is vertical along the column-segment axis, perpendicular to the x_i-y_i plane. The member paralled to the undisturbed free surface is called a hull, and that normal to the undisturbed free surface is called a column. The subscript "c" stands for a column, the subscript "h" stands for a hull, and the subscript "i" stands for the i^{th} segment. There is a segment-orientation angle γ_i in the horizontal ($x-y$) plane between the x-and x_i-axes for a hull which is not parallel to the x-axis for many existing semisubmersible drilling rigs, $\gamma_i \neq 0$.

Let $\xi(t)$, $\eta(t)$, and $\zeta(t)$ be the time-dependent, oscillatory, translatory displacements of the structure's CG with reference to their mean value of the body(x,y,z) coordinate system and correspond to surge, sway, and heave, respectively. Let $\phi(t)$, $\theta(t)$, and $\psi(t)$ be the time-dependent, oscillatory, angular displacements about the structure's CG, corresponding to roll, pitch, and yaw, respectively. Then the translatory displacements of the i^{th} segment located at a point (x_{ci}, y_{ci}, z_i) can be written in terms of the displacements for the structure's CG,

$$\xi_i(t)=[\xi(t)+z_i\theta(t)-y_{ci}\psi(t)]\cos\gamma_i + [\eta(t)+x_{ci}\psi(t)-z_i\phi(t)]\sin\gamma_i \quad (1)$$

$$\eta_i(t)=[\eta(t)+x_{ci}\psi(t)-z_i\phi(t)]\cos\gamma_i - [\xi(t)+z_i\theta(t)-y_{ci}\psi(t)]\sin\gamma_i, \quad (2)$$

$$\zeta_i(t)=\zeta(t)+y_{ci}\phi(t)-x_{ci}\theta(t) \quad (3)$$

The nonsubscribed displacements in (1) to (3) are the motion displacements of or about the structure's CG relative to its position in the undisturbed free surface.

Indeed $\xi_i(t)$, $\eta_i(t)$, and $\zeta_i(t)$, (1) to (3) are the motion displacements of any point rigidly oscillating with the motions of the structure in waves in the x_i-, y_i-, and z_i -directions, respectively. The motion displacements of a point, (1), (2), and (3) are expressed in terms of the six degrees of motion of the structure which are to be calculated by the method presented in the text. Once the six degrees of motion are computed with the forces acting on the individual segment points, motions of the segment points, (1), (2), and (3) rigidly oscillating with the structure motion can be computed.

It is assumed that the responses of the structure are linear and harmonic. Then six linear coupled differential equations of motion can be written,

$$\sum_{k=1}^{6}[(M_{jk}+A_{jk})\ddot{x}_k+B_{jk}\dot{x}_k+C_{jk}x_k]=F_je^{i\omega t} \quad (4)$$

where

$$x_k(t)=\begin{cases}\xi(t) & \text{surge}\\ \eta(t) & \text{sway}\\ \zeta(t) & \text{heave}\\ \phi(t) & \text{roll}\\ \theta(t) & \text{pitch}\\ \psi(t) & \text{yaw}\end{cases}, \quad j=1,2.\ldots 6. \quad (5)$$

and M_{jk} are the components of the generalized mass matrix for the structure, A_{jk} and B_{jk} are the added mass coefficients and damping coefficients, respectively, C_{jk} are the hydrostatic restoring coefficients, and F_j are the exciting forces and moments. F_1, F_2, and F_3 are

the amplitudes of the surge, sway, and heave exciting forces, while F_4, F_5 and F_6 are the amplitudes of the roll, pitch and yaw exciting moments. The dots stand for time derivatives so that $\dot{x}_k$ and $\ddot{x}_k$ stand for velocity and acceleration terms.

The rig CG is located at the origin of the (x, y, z) coordinate. The generalized mass matrix of the rig is given by

$$M_{jk}=\begin{pmatrix} M & 0 & 0 & 0 & 0 & 0 \\ 0 & M & 0 & 0 & 0 & 0 \\ 0 & 0 & M & 0 & 0 & 0 \\ 0 & 0 & 0 & I_4 & 0 & -I_{46} \\ 0 & 0 & 0 & 0 & I_5 & 0 \\ 0 & 0 & 0 & -I_{46} & 0 & I_6 \end{pmatrix} \quad (6)$$

where M is the mass of the rig, I_j is the moment of inertia in the j^{th} mode ($j=4, 5$, and 6), and I_{jk} is the product of inertia. The roll-yaw product I_{46} vanishes if the structure has fore-and-aft symmetry and is small otherwise: many recently built drilling rigs have their derrick very close to the rig CG, $I_{46}=0$ Other components (6) vanish, since the origin of the coordinate system (Figs. 1 and 2) is the same as the rig CG.

The added-mass (or damping) coefficients for the rig are

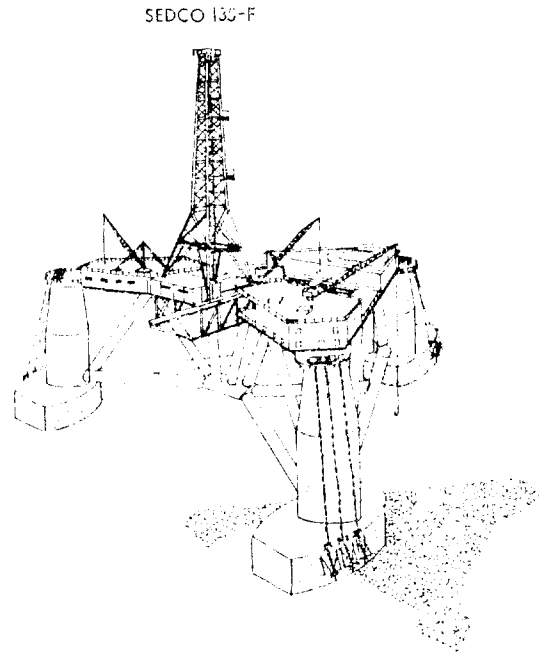

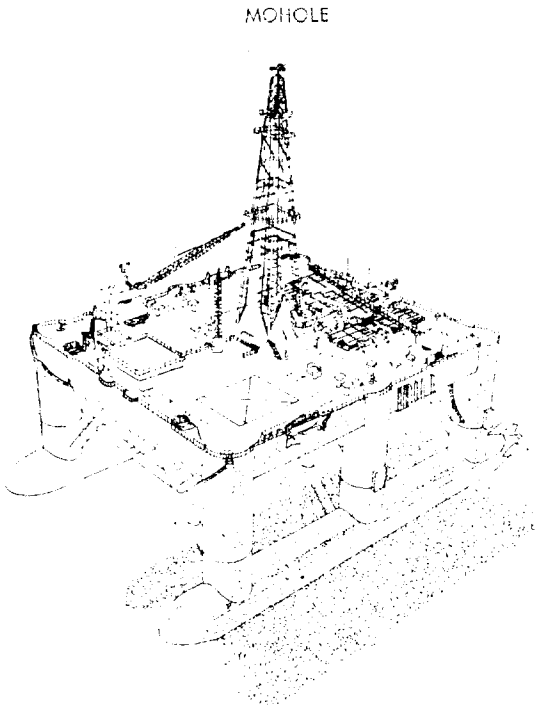

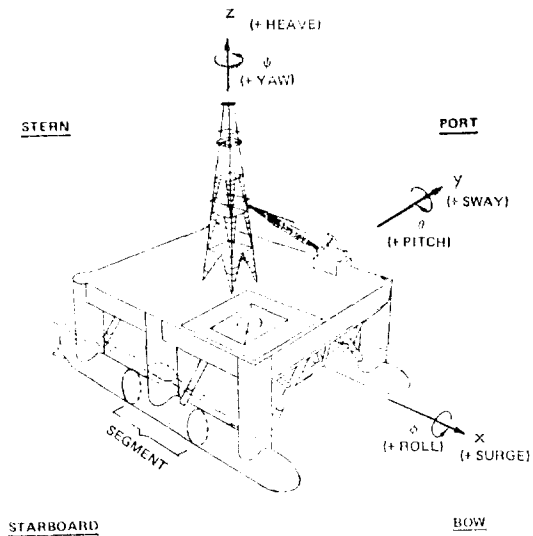

Fig. 1. -Sketch of SEDCO 135-F Rig and the MOHOLE Rig and the Coordinate Systems.

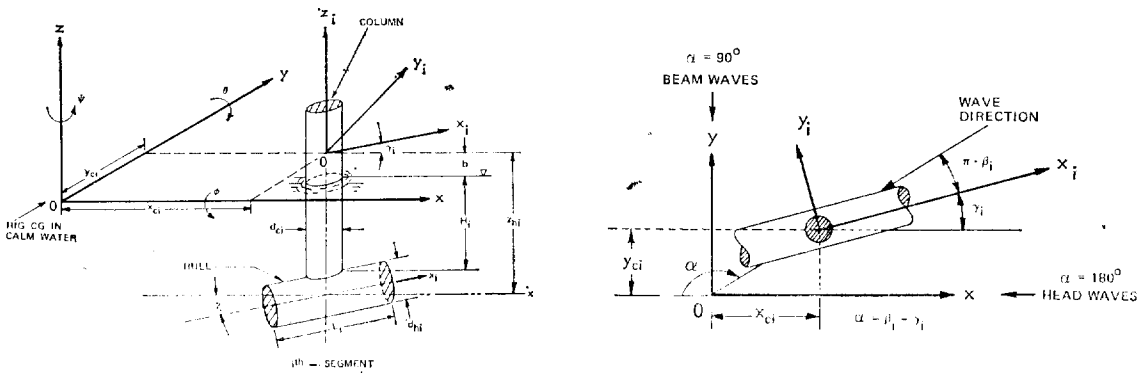

Fig. 2. The Coordinate Systems of the Rig Segments.

$$A_{jk}=(\text{or } B_{jk})=\begin{pmatrix} A_{11} & A_{12} & 0 & A_{14} & A_{15} & A_{16} \\ A_{21} & A_{22} & 0 & A_{24} & A_{25} & A_{26} \\ 0 & 0 & A_{33} & A_{34} & A_{35} & 0 \\ A_{41} & A_{42} & A_{43} & A_{44} & A_{45} & A_{46} \\ A_{51} & A_{52} & A_{53} & A_{54} & A_{55} & A_{56} \\ A_{61} & A_{62} & 0 & A_{64} & A_{65} & A_{66} \end{pmatrix} \quad (7)$$

For the stationary (or zero forward speed) rig the coefficients (7) are symmetric; $A_{jk}=A_{kj}$ and $B_{jk}=B_{kj}$. Unlike for a monohull body [14], the added mass coefficients and the damping coefficients are additionally coupled between the modes of sway-surge, roll-surge, yaw-surge, surge-sway, heave-roll, pitch-sway, pitch-roll, and yaw-pitch. The couplings for these coefficients exist due to the fact that some of the member segments are not parallel to the x-axis for many floating structures for which the submerged portion is not symmetric about the x-and y-axis. For floating rigs such as MOHOLE [4], the member segments are parallel to the x-axis, or $\gamma_i=0$ and also has a lateral symmetry [8, 15]; consequently, $A_{12}=A_{14}=A_{16}=A_{25}=A_{45}=A_{56}=A_{34}=0$, and similarly for the corresponding B_{jk}. The special case of $\gamma_i=0$ includes Reference [11]: References [3, 12]^{jk} are not specific enough to distinguish the cases.

Furthermore, the hydrostatic restoring coefficients for the rig are

$$C_{jk}=\begin{pmatrix} 0 & 0 & 0 & 0 & 0 & 0 \\ 0 & 0 & 0 & 0 & 0 & 0 \\ 0 & 0 & C_{33} & C_{34} & C_{35} & 0 \\ 0 & 0 & C_{43} & C_{44} & C_{45} & 0 \\ 0 & 0 & C_{53} & C_{54} & C_{55} & 0 \\ 0 & 0 & 0 & 0 & 0 & 0 \end{pmatrix} \quad (8)$$

Also the hydrostatic restoring coefficients have a property of symmetry; $C_{jk}=C_{kj}$. The hydrostatic restoring coefficients are independent of frequency and segment-orientation angle, γ_i. For the case of a lateral symmetry [8, 18], $C_{34}=C_{45}=0$.

The coefficients A_{jk}, B_{jk}, C_{jk}, (7) and (8) and the exciting forces and moments F_j (j, $k=1,2...6$) are derived later in detail: these are first derived in the segment (x_i, y_i, z_i) coordinate system for j, $k=1,2,3$ and are transformed to the body (x,y,z) coordinate system for $j,k=1,2....6$. It should be noted that A_{jk}, B_{jk}, C_{jk} and F_j can each take into account pairs of column and hull segments.

The coefficients, (7) and (8) indicate coupling between nearly all six modes of motion displacements except between surge-heave, sway-heave, and heave-yaw. Therefore all six equations of motion (4) must be simultaneously solved with the coefficients, (7) and (8) and the exciting forces and moments to get the motions (5). The numerical computions are discussed later in detail. In order to get the coefficients, (7) and (8) and the exciting forces and moments, the total forces will be derived in the next.

3. Formulation of Equations of Total Forces

3.1 General Descriptions

Total force on the submerged portion of a segment located at a point (x_{ci}, y_{ci}, z_i) in the segment (x_i, y_i, z_i) coordinate system consists of: (1) Froude-Krilov force; the force due to the undisturbed waves acting on the segment in its mean position, (2) "diffraction"

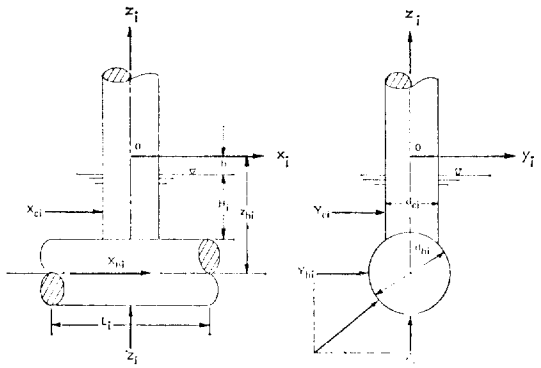

Fig. 3. Force Components on the i^{th} Segment in the x-, y-, and z-directions.

force; the force due to the waves disturbed by the presence of the segment in its mean position; this force is a correction for the the disturbances to the Froude-Krilov force, (3) "motion-dependent" force; the force due to the motions of the segment rigidly oscillating with the rig, and (4) hydrostatic forces; the forces consist of the force due to the wave surface variation along the segment, the force due to the buoyancy variation of the waterplane area due to the rig or segment motion, and the buoyancy force. The first two hydrostatic force components are included in the derivation of the Froude-Krilov force for convenience, and the buoyancy force is included directly in the equations of motion which are discussed following the forces.

The "wave force" consists of the Froude-Krilov force and the "diffraction" force, and the terminology "wave force" is used throughout this paper following its common usage in the offshore engineering industry. The "wave" force is the same terminology in this paper as the exciting force. The hydrodynamic force consists of the wave force and the "motion-dependent" force, but also includes the hydrostatic forces in the derivations for convenience.

We shall discuss the total forces in two coordinate systems: the total forces in the segment (x_i, y_i, z_i) coordinate system as described above and the total forces in the body (x, y, z) coordinate system. The total forces on many individual rig-member segments in the segment coordinate system can be used as total force distribution along the rig members. With an increase in the number of the segments, finer total force distribution along the rig members can be obtained. The total force distribution is an important input information for the structural analysis of a rig. The structural analysis would require additional inputs of wind force, current forces and mooring line effect. The "total force" terminology here does not include the above additional force components. The forces on the segments derived in the segment coordinate can be transformed to the forces in the body coordinate system which, when summed over all the segments, give the total forces on the entire rig in the body coordinate system. The total forces on the entire rig in the body coordinate system can be used for the derivation of the hydrodynamic and hydrostatic coefficients and the exciting forces and moments from the equations of motion (91) to (96).

These forces are derived for finite depth, but are also applicable to infinite depth. The infinite depth problem [4] is already solved.

3.2. Mathematical Approach

The present approach for the derivation of the hydrodynamic force in the (x, y, z) coordinate system uses potential flow theory for zero forward speed and leads to the forms [1, 3, 4, 6, 11, 12, 20] of the equations of the hydrodynamic forces by the other approach. The other approach has been applied by Bain [1] for the floating rig problem and later by many others. The other approach is to use the available method of starting with the inertia force which is the virtual mass multiplied by the particle acceleration and the damping force, and has commonly been used in principle by the coastal engineering field [7, 20].

There has been a little confusion on the clear differences and similarity between the two approaches. These two approaches are compared and are shown to be the same with minor assumptions involved. We shall begin with an approach similar to potential flow theory for the ship motion problem with zero forward speed used by Salveson, et al [14] and lead it to the forms of the force equations used by the other approach.

The linearized velocity potential $\Phi(x, y, z; t)$ satisfies the Laplace equation,

$$\nabla^2\Phi(x, y, z, t)=0 \quad \text{in the fluid} \tag{9}$$

The velocity potential (9) must satisfy the linearized

boundary condition on the free surface ($z=-b$),

$$\Phi(x,y,-b;t)+g\frac{\partial\Phi}{\partial z}(x,y-b,t)=0 \tag{10}$$

and the boundary condition of uniform bottom($z=-b-h$)

$$\frac{\partial\Phi}{\partial z}(x,y,-b-h;t)=0 \tag{11}$$

where

g=gravity acceleration

h=water depth of uniform bottom.

The free surface condition (10) with the bottom condition (11) then becomes for finite depth,

$$\frac{\omega^2}{g}=k\tanh kh \tag{12}$$

where

ω=circular wave frequency in rad/sec and is the same as the frequency of the rig response in waves

k=wave number

For "shallow" depth, $kh\to 0$ and consequently $\tanh kh \approx kh$, then the relationship (12) becomes

$$\frac{\omega^2}{g}=k^2h \tag{13}$$

For "infinite" depth, $kh\to\infty$ and consequently $\tanh kh \approx 1$, then the relationship (12) becomes

$$\frac{\omega^2}{g}=k \tag{14}$$

For an easy reference, Tables 1 and 2 provide wave classification according to relative depth and asymptotes of wave functions, respectively. The relative depth is defined as ratio of the water depth h to the wavelength λ.

Table 1. Wave Classification According to Relative Depth

Range of h/λ	Range of $kh=2\pi h/\lambda$	Types of Waves
0 to 1/20	0 to $\pi/10$	"shallow water" waves (long waves)
1/20 to 1/2	$\pi/10$ to π	"intermediate depth" waves
1/2 to ∞	π to ∞	"deep water" waves (short waves)

Table 2. Asymptotes of Wave Functions

Function	Asymptotes	
	Shallow Water	Deep Water
sinh kh	kh	$e^{kh}/2$
cosh kh	1	$e^{kh}/2$
tanh kh	kh	1

Let the linearized velocity potential for zero forward speed be

$$\Phi(x,y,z,t)=\phi_t(x,y,z)e^{i\omega t} \tag{15}$$

For the present purpose the amplitude of the time-independent part of the unsteady velocity potential is linearly decomposed,

$$\phi_t=\phi_I+\phi_D+\sum_{j=1}^{3}x_j\phi_j \tag{16}$$

where

ϕ_I=incident wave potential

ϕ_D=diffraction potential

x_j=the jth mode of motion displacement

ϕ_j=the contribution to the velocity potential from the jth mode of motion

The incident waves diffract upon the body and scatter in all directions. Also the incident waves set the body into motion and the motion of the body generates additional waves in all directions. The notation $\phi(t)$ without a subscript is used to represent the roll motion, and the equation (16) represent the potentials for ϕ with subscripts

In addition to the Laplace equation (9), the free surface condition (10), the bottom condition (11) and the relationship (12), the velocity potentials (16) should each satisfy the appropriate boundary condition at infinity. Also ϕ_I and ϕ_D must satisfy the body surface boundary condition

$$\frac{\partial\phi_I}{\partial n}=-\frac{\partial\phi_D}{\partial n} \text{ on the segment at mean position} \tag{17}$$

Also the oscillatory potential components, $\phi_j(j=1,2,3)$ must satisfy the body surface condition,

$$\frac{\partial\phi_j}{\partial n}=i\omega n_j \text{ on the segment oscillating in mode j} \tag{18}$$

where the generalized normal, n_j, is defined by

$$(n_1,\ n_2,\ n_3)=\bar{n} \tag{19}$$

with $\bar{n}$ the outward unit normal vector and $j=1,2,3$.

The velocity potential (15) can be used to get the first order approximation of pressure from Bernoulli equation,

$$p(x,y,z;t)=-\rho gz-\rho\dot{\Phi}(x,y,z,t) \tag{20}$$

where ρ=fluid density.

Let the pressure distribution at the free surface be

$p=0$, then the wave-surface profile can be written in terms of the velocity potential (15),

$$\bar{\zeta}(x.y;t)=-\frac{1}{g}R_e\ \{\dot{\phi}(x,y,-b,t)\}$$
$$=A\ \cos(k_1x-k_2y-\omega t) \qquad (21)$$

or

$$\bar{\zeta}(x_i,y_i;t)=\zeta_i(t)+\bar{\zeta}(x,y;t)$$

where

A=wave amplitude

$k_1=k\ \cos\ \beta_i$

$k_2=k\ \sin\ \beta_i$

$\beta_i=\alpha+\gamma_i$

γ_i=angle of the incident wave direction relative to the x axis in the x-y plane, or angle between the x- and x_i- axes.

α=angle of the incident wave direction relative to the x-axis in the x-yplane ($\alpha=\pi/2$ for beam waves, and $\alpha=\pi$ for head waves)

$\bar{\zeta}(x,y;t)$ is a single harmonic progressive wave, $\bar{\zeta}(x_{ci}, y_{ci};t)$ is the corresponding wave in the (x_i, y_i, z_i) coordinate, and the vertical motion of the i^{th} segment, $\zeta_i(t)$, is defined by (3). The diameters or cross-sectional dimensions of the hull and column segments of the rig will later be assumed to be small compared to the incident wavelength. Consequently the motion of the wave surface is assumed to be uniform across the cross-sectional surface of the segment about the waterplane center of the segment.

The subsurface presure (for $z_i<\bar{\zeta}$)on the i^{th} segment point in the (x_i, y_i, z_i) coordinate system can be written with the equations (9), (12) and (15),

$$p_i(x_i, y_i, z_i;t)=-\rho g[\zeta_i(t)+z_i]-\rho\dot{\phi}(x_i, y_i, z_i;t) \quad (22)$$

We shall stay in the segment (x_i, y_i, z_i) coordinate system from here on until when otherwise stated.

Integration of the pressure (22) over the i^{th} segment surface gives the wave force

$$(x_j)_i e^{i\omega t}=-\rho\iint_{s_i} n_j(\dot{\phi})_i ds_i \qquad (23)$$
$$j=1,2,3$$

where the subscript i indicates the i^{th} segment.

s_i is the surface of the i^{th} segment, and j indicates the direction of the force x_j. Hydrostatic restoring force resulting from the pressure (22) is ignored here and is retained later. It is also reminded that N number of segments constitute the submerged portion of the floating rig.

By applying equation (16) to the force (23) the linear total force on the i^{th} segment can be divided into three parts as

$$(X_j)_i=-i\rho\omega\iint_{s_i} n_j(\phi_I+\phi_D+\sum_{k=1}^{3}x_k\phi_k)_i ds_i$$
$$=X_j^{F-K}+X_j^D+X_j^M \qquad (24)$$

where

$$X_j^{F-K}=-i\rho\omega\iint_{s_i}\phi_I\ \cos\ (n,x_j)\ ds_i \qquad (25)$$

$$X_j^D=-i\rho\omega\iint_{s_i}\phi_D\ \cos\ (n,x_j)\ \mathrm{d}s_i \qquad (26)$$

$$X_j^M=-i\rho\omega\iint_{s_i}\sum_{k=1}^{3}x_k\phi_k\ \cos\ (n,x_j)\ ds_i \qquad (27)$$

The subscript i denoting the i^{th} segment will be dropped from here on unless essentially necessary, and the equations from (24) on are referred to the i^{th} segment in the $(x_i,\ y_i,\ z_i)$ coordinate system. X_j^{F-K} (25) is the Froude-Krilov force, X_j^D (26) is the diffraction force, and X_j^M is the motion-dependent force in still water: these forces act on the i^{th} segment in the j^{th} direction; x_i for $j=1$, y_i for $j=2$, and z_i for $j=3$. As described before the wave force consists of the Froude-Krilov force and the diffraction force.

3.3. Wave Forces

3.3.1. Foroude-Krilov Force

The force from the pressure distribution equal to the force due to the undisturbed waves acting on the segments in the mean position is called Froude-Krilov force.

The linear velocity potential for an incident, single harmonic progressive wave (15) can be written for finite depth,

$$\phi_I=\frac{igA}{\omega}\ \frac{\cosh\ k(z+h+b)}{\cosh\ kh}\exp$$
$$[-i(k_1x-k_2y-\omega t)] \qquad (28)$$

The quantity $\cosh\ k(z+h+b)/\cosh\ kh$ is usually called the "pressure response factor", and is less than unity for all depths below the mean free surface. Equation (28) does not yet but satisfy the relationship (12).

The subsurface pressure (22) with the incident wave potenial (28) for the the i^{th} segment in the (x_i, y_i, z_i) coordinate system becomes

$$p_i=\rho\{-g[\zeta_i(t)+z_i]$$
$$+\frac{\omega^2A}{k}\ \frac{\cosh\ k(z_i+h+b)}{\sinh\ kh}\exp[-i(k_1x_i-k_2y_i-\omega t)]\} \qquad (29)$$

The last term of the pressure (29) satisfies the relationship (12).

The Froude-Krilov force (25) for the (x_i,y_i,z_i) coordinate system can be written in different expressions,

$$X_j^{F-K}=-i\omega\rho\iint_{s_i}n_j\phi_I ds_i \tag{30-a}$$

$$X_j^{F-K}e^{i\omega t}=-\rho\iiint_{V_i}\dot{v}_j dV_i \tag{30-b}$$

$$=\iiint_{V_i}\frac{\partial p_i}{\partial x_j}dV_i \tag{30-c}$$

where

s_i=surface per unit length of the i^{th} segment

V_i=volume of the i^{th} segment

$x_j=(x_i,y_i,z_i)$.

Gauss' theorem is applied to change the surface integral (30-a) to the volume integral (30-b). The present approach uses the expression (30-b) or (30-c) to get the Froude-Krilov forces. The expression (30-a) is used by Kim [8] for the motions of a rig in deep water and by Salveson, et al [14] for the ship motion problem.

The water-particle orbital velocity with the velocity potential and the relationship (30) is

$$\dot{x}_j=v_j=\frac{\partial\Phi_I}{\partial x_j} \tag{31}$$

$\dot{x}_j$ is the time derivative of the particle displacement in the j-direction,

The time derivative of the particle orbital velocity (31) gives the particle orbital acceleration,

$$v_j=\frac{\partial}{\partial t}\left(\frac{\partial\Phi}{\partial x_j}\right)=\frac{\partial\dot{\Phi}_I}{\partial x_j} \tag{32}$$

which leads the equation (32) with Gauss' theorem to the form (30-b).

The derivation of expression (30-c) can be obtained with the pressure (22) (ignoring the hydrostatic restoring force) and the acceleration (32),

$$-\frac{\partial p_i}{\partial x_j}=\rho\frac{\partial\dot{\Phi}_I}{\partial x_j} \tag{33}$$

Applying the expressions (30-b) and (30-c), the Froude-Krilov force on the i^{th} segment including the hydrostatic force (29) can be written

$$X_j^{F-K}e^{i\omega t}=-\rho\iiint v_i\{g\frac{\partial}{\partial x_j}[\zeta_i(t)+z_i]+\dot{v}_j\}dVi \tag{34}$$

The hydrostatic term can be obtained from the pressure (29), and the particle acceleration is given by equation (32). Up to this point, there has been no additinal assumptions involved to those made for equations (30). In the next we shall make a few minor assumptions to equation (34), and the resultant equations will be more convenient to use for the numerical computation without causing any significant numerical accuracy problem for a floating structure or rig.

The submerged portions of the segments and the submerged member segments of the majority of the existing floating rigs have their cross-sectional dimension or diameter very small compared to the wavelength. So we shall make a few consequent, reasonable *assumptions*, that the rig consists of many segments, small compared to the wavelength and water depth, that the pressure acts on the displaced-fluid mass centers of the segments, and that the motion of the wave surface is uniform across the cross-sectional surface of the segment about the waterplane center of the segment. The segment can be either hull (horizontal) or column (vertical). The first assumption implies that $kx_i\ll 1$, $ky_i\ll 1$ for the column and $ky_i\ll 1$ and $kz_i\ll 1$ for the hull and $kh=0(1)$. It is noted that the references [3, 6, 12] failed to point out the assumption that the cross-sectional dimension of the segment is small compared with the water depth for their equations of finite depth.

With the above assumptions the Froude-Krilov force (34) can be written

$$X_j^{F-K}e^{i\omega t}=-\rho gA_{wpi}(\zeta_i(t)-\bar{\zeta})\delta_{33}+\rho\frac{A_i}{\bar{x}_L}\cdot\int\dot{v}_j dx_L \tag{35}$$

where δ_{33}=dirac delta function

A_{wpi}=waterplane area of the i^{th} segment

$\bar{\zeta}(x_{ci},y_{ci};t)$=wave-surface profile at the i^{th} segment point $(x_{ci},y_{ci},-b)$

dx_L=length variable along the axis of the segment

$\bar{x}_L$=length of the segment

Also the assumptions that the cross-sectional dimension of the segment is small compared with the wavelength and water depth and that the pressure acts on the displaced-fluid mass point of the segment allow to change the volume integral (34) to the line integral (35) by taking the area A_i outside the integral (35). This also means that A_i is independent of x_L for the cylinder segment of which the cross-sectional geometry

does not vary along x_L. However, the dependence of A_i on x_L can be restored by increasing the number of segments for a given member length with as much accuracy as the strip theory principle gives; the effect of the axial variation of the coss-sectional geometry of the member is ignored. The integration range in the second term (35) is discussed later. For the numerical computations of the forces and motions keeping the area A_i outside the integral (35) gives an easier data handling and perhaps shorter computer running time.

Thus a final form of the Froude-Krilov force (35) on the i^{th} segment can be written

$$X_j^{F-K} e^{i\omega t} = -\rho g A_{wpi}(\zeta_i(t)-\bar{\zeta})\delta_{33} + \frac{m_i}{\bar{X}_L}\int \dot{v}_j dx_L \tag{36}$$

where $m_i=\rho A_i \bar{X}_L$. There are only vertical directional hydrostatic forces. Buoyancy force will reappear in the equations of motion.

The expression (36) was first applied by Bain [1] for the floating platform problem during the development of project MOHOLE, and later by others [3, 4, 6, 11, 12,]. The expression (30-a) for the Froude-Krilov force differs from the expression (36) by the resulting difference due to the above assumptions applied to get the expression (36) form (30-b) or (30-c) which is equivalent to the expression (30-a). As will be discussed later, this resulting difference seems to be little for the numerical computational accuracy. The expression (30-a) was applied to the floating platform problem by Kim [8] without being related to (30-b) or (30-c) and is commonly used for the ship motion problem [14]. Without applying potential flow theory the expression (36) has been used by Bain [1], Burke [3], Ochi [11], and Hooft [6] and the offshore petroleum industry for the floating platform motion problems. Paulling [12] derives the expression (36) from the expression (30-c) with the hydrostatic force terms separately treated. Chung [4] derives the expression (36) from the expression (30-c). The works by both Paulling [12] and Chung [4] are also similar to Bain [1].

Thus the Froude-Krilov force (30-a) is the same as (36) except the resulting difference due to the assumptions applied to (30) to get the expression (36). So far there has been made little clarification to distinguish the expression (30) from the expression (36) for the floating platform motions. It is noted that the paper using the expression (36) all failed to state the assumption that the cross-sectional dimension of the segment is small compared to the water depth, even though the equations for the finite depth [3, 6, 12] were used.

It is also noted that although the equations for the finite depth were used by these papers, only Burke [3] presents numerical computations of six degrees of motion, and Hooft [6] computed numerical computations for heave, roll and pitch motions and the exciting forces.

For example of details of equation (36) the y_i-directional component of the Froude-Krilov force on the i^{th} *hull* segment, Y_{hi}^{F-K} will be derived as follows.

The y_i-directional water particle velocity at the displaced-mass point of the i^{th} hull segment, (x, y_{ci}, z_i) is from (31),

$$v_{hyi} = -\omega A \frac{\cosh k(z_i+h+b)}{\sinh kh}\sin\beta_i \; exp[-i(k_1 x - k_2 y_{ci} - \omega t)] \tag{31}$$

which satisfies the relationship (12), and $x=x_{ci}+x_i$.

The y_i-directional water particle acceleration corresponding to the particle velocity (31) is the time derivative of the velocity (31),

$$\dot{v}_{hyi} = -i\omega^2 A \frac{\cosh k(z_i+h+b)}{\sin hk}\sin\beta_i \; exp[-i(k_1 x - k_2 y_{ci} - \omega t)] \tag{32}$$

Substitution of the water particle acceleration (32) at (x, y_{ci}, z_i) into equation (36) gives y_{hi}^{F-K} which acts on the displaced-mass center of the i^{th} hull segment,

$$Y_{hi}^{F-K} e^{i\omega t} = \frac{m_{hi}}{L_i}\int_{-\frac{L_i}{2}}^{\frac{L_i}{2}} \dot{v}_{hyi} dx_i \tag{37}$$

where

m_{hi}=displaced mass of water by the i^{th} hull segment $(=\rho A_{hi} L_i)$

A_{hi}=cross-sectional area of the i^{th} hull segment

L_i=length of the i^{th} hull segment.

A Procedure similar to that used above for the hull (37), the y_i-directional component of the Froude-Krilov force on the i^{th} *column* segment, Y_{ci}^{F-K} can be derived as follows,

$$Y_{di}^{F-K} e^{i\omega t} = m_{ci}\frac{1}{H_i}\int_{-(Hi+b)}^{-b} \dot{v}_{cyi} dz_i \tag{38}$$

where

m_{ci}=displaced-water mass by the i^{th} column segment($=\rho A_{ci}H_i$)

A_{ci}=cross-sectional area of the i^{th} column segment

H_i=length of the submerged portion of the i^{th} column segment.

The integration for the equation should be carried out along the vertical direction to the free surface.

Similarly, the x_i-directional component of the forces, X_{hi}^{F-K} on the i^{th} hull and X_{ci}^{F-K} on the i^{th} column, and the z_i-directional component of the forces, Z_{hi}^{F-K} on the i^{th} hull and Z_{ci}^{F-K} on the i^{th} column can be obtained with the equation (36).

Thus the Froude-Krilov forces on the i^{th} column and hull segments are summarized in the following. Taking Re $[X_j^{F-K}e^{i\omega t}]$ gives

$$X_{ci}^{F-K}=m_{ci}\omega^2AQ_o(k)\cos\beta_i\sin\tau_i \tag{39}$$

$$Y_{ci}^{F-K}=-m_{ci}\omega^2AQ_o(k)\sin\beta_1\sin\tau_i \tag{40}$$

$$Z_{ci}^{F-K}=-(m_{ci}\omega^2P_o(k)-\rho gA_{cwi})A\cos\tau_i-\rho gA_{cwi}\zeta_i \tag{41}$$

$$X_{hi}^{F-K}=m_{hi}\omega^2AI_{si}(k)\cos\beta_1 \tag{42}$$

$$Y_{hi}^{F-K}=-m_{hi}\omega^2AI_{si}(k)\sin\beta_1 \tag{43}$$

$$Z_{hi}^{F-K}=-m_{hi}\omega^2AJ_{ci}(k)+\rho gA_{hwi}(A\cos\tau_i-\zeta_i) \tag{44}$$

The notations used for the above equations are defined as follows:

$$\tau_i=k_1x_{ci}-k_2y_{ci}-\omega t \tag{45}$$

$$Q_o(k)=\frac{1}{kH_i}\int_{-(H_i+b)}^{-b}\frac{\cosh k(z_i+h+b)}{\sinh kh}dz_i \tag{46}$$

$$P_o(k)=\frac{1}{kH_i}\int_{-(H_i+b)}^{-b}\frac{\sinh k(z_i+h+b)}{\sinh kh}dz_i \tag{47}$$

A_{cwi}=waterplane area of the i^{th} column segment

$$\zeta_i=\zeta+y_{ci}\phi-x_{ci}\theta \tag{3}$$

$$\frac{I_{si}}{I_{ci}}(k)=\frac{1}{kL_i}\frac{\cosh k(-H_i-d_{hi}/2+h)}{\sinh kh}X\int_{-L_i/2}^{L_i/2}\frac{\sin}{\cos}\{k_1(x_{ci}+x_i)-k_2y_{ci}-\omega t\}dx_i \tag{48}$$

$$\frac{J_{si}}{J_{ci}}(k)=\frac{\sinh k(-H_i-d_{hi}/2+h)}{\cosh k(-H_i-d_{hi}/2+h)}\frac{I_{si}}{I_{ci}}(k) \tag{49}$$

A_{hwi}=waterplane area of the i^{th} hull segment.

The relationships (39) to (49) are valid for both finite and infinite depths. The relationships (46) to (49) for the case of the infinite depth only are separately defined in Reference [4]. Except for the difference in these relationships, the Froude-Krilov force equations (39) to (44) are essentially the same for the cases of the finite depth and infinite depth. The hydrostatic restoring forces appear in the equations (41) and (44). For the hull (41), the first hydrostatic restoring term is the wave-surface motion effect on the i^{th} column segment, and the second hydrostatic restoring term is due to the vertical motion (heave, roll, and pitch) of the waterplane area of the i^{th} column segment. Note that the wave-surface motion is assumed to be uniform across the waterplane center of the segment for the instant waterline. The hydrostatic term for the column (44) is due to the wave-surface motion on the hull segment and the vertical motion of the waterplane area of the i^{th} hull if emerged in the free surface. For the majority of the existing semi-submersible drilling rigs for the drilling operational mode, usually the hulls are completely submerged, or $A_{hwi}=0$.

Similar procedure is applied to derive the diffraction force for which the diffraction potential can be connected to the undisturbed incident wave potential used to get the Froude-Krilov force.

3.3.2. Diffraction Force

The incident waves are indeed disturbed by the presence of the rig-member segments, and this disturbance requires a correction to the Froude-Krilov force derived above. This correction part of the force will be called the forces due to the diffracted waves or the "diffraction" force. The procedure to get the diffraction force is similar to that for the Froude-Krilov force (30-b, 30-c), is derived with potential flow theory, and is shown to be identical with the equations by the different approach discussed above under the same assumptions used for the Froude-Krilov force (36). Again we shall discuss this problem in the (x_i, y_i, z_i) coordinate only.

The diffraction force (26) with the body condition (18) is

$$X_j^D=-\rho\iint_{s_i}\frac{\partial\phi_j}{\partial n}\phi_D ds_i,\qquad j=1,2,3 \tag{50}$$

Using Green's second identity, equation (50) becomes

$$X_j^D=-\rho\iint_{si}\phi_j\frac{\partial\phi_D}{\partial n}ds_i \tag{51}$$

Then use of the body boundary condition (17), i.e.

$$\frac{\partial \phi_D}{\partial n}=-\frac{\partial \phi_I}{\partial n} \quad \text{on the segment surface at mean position} \tag{17}$$

shows that the diffraction force becomes

$$X_j^D=\rho \iint_{s_i} \phi_j \frac{\partial \phi_I}{\partial n} ds_i \tag{52}$$

where

$$\frac{\partial \phi_I}{\partial n}=(-in_1 \cos \beta_i + in_2 \sin \beta_i + n_3) k \phi_I \tag{53}$$

$ds_i = dx_L dl_i$

dl_i = element of arc along the cross section C_x.

Applying the same assumptions used to change the form (30-b) to the Froude-Krilov force (36), the water-particle velocity at the displaced-mass-water point (x_{ci}, y_{ci}, z_i) of the i^{th} segment can be assumed to be independent of the added mass coefficients and damping coefficients, t_{jk}. Then equation (52) can be expressed as,

$$X_j^D=-\left[\sum_{k=1}^{3} \int_{L_i} dx_L \frac{\partial \phi_I}{\partial x_k} \int_{C_x} i\rho\omega n_k \phi_j dl_i\right] \frac{1}{i\omega}$$

$$X_j^D e^{i\omega t}=-\left[\sum_{k=1}^{3} t_{jk} \int_{L_i} v_k \, dx_L\right] \frac{1}{i\omega} \tag{54}$$

where

$$t_{kj}=-i\rho\omega \int_{C_x} n_k \phi_j dl_i = \omega^2 a_{kj} - i\omega b_{kj}. \tag{55}$$

$j, k = 1, 2, 3.$

The particle velocity v_k is defined by (31). C_x is any cross section. a_{kj} and b_{kj} are the two-dimensional, segmental added mass coefficients and damping coefficients, respectively in the (x_i, y_i, z_i) coordinate system, not in the (x, y, z) coordinate system. Here for $j \neq k$, $a_{kj}=0=b_{kj}$ $(j, k=1, 2, 3)$ for the cylinder segment of constant cross-sectional shape along its length: for the case [6] of arbitrary hull form as his coordinate axes are defined, $a_{jk} \neq 0 \neq b_{jk}$ contrary to his general application of $a_{jk}=0=b_{jk}$ without a proper justification, when $j \neq k$. This argument also applies to the footing of the SEDCO 135-F rig as described later for the motion computations.

The "diffraction" force X_j^D (54) on the i^{th} segment in the (x_i, y_i, z_i) coordinate system with the relationship (55) can be expressed in two parts; the forces associated with the particle acceleration and the forces associated with the particle velocity.

For the $j=2$ mode $\left(Y_{hi}^D=(X_2^D)_{hull}\right)$ on the i^{th} *hull* segment, the diffraction force (54) becomes

$$Y_{hi}^D e^{i\omega t}=-\Big[(\omega^2 a_{12}-i\omega b_{12})_{hi} \int_{L_i} v_{hzi} dx_i + (\omega^2 a_{22}-i\omega b_{22})_{hi} \int_{L_i} v_{hyi} dx_i + (\omega^2 a_{32}-i\omega b_{32})_{hi} \int_{L_i} v_{hzi} dx_i\Big] \frac{1}{iw} \tag{56}$$

Since $a_{12}=a_{32}=b_{12}=b_{32}=0$ for the i^{th} cylinder segment in the (x_i, y_i, z_i) coordinate system, the x_i-directional "diffraction" force (56) with the relationship (31) and (32) can be divided into the acceleration term and the velocity term,

$$Y_{hi}^D e^{i\omega t}=(a_{22} \int \dot{v}_{hyi} dx_i + b_{22} \int v_{hyi} dx_i)_{hi} \tag{57}$$

The subscript *hi* on the right-hand side of equation (57) denotes the i^{th} hull, and later the i^{th} colum will be denoted as subscript *ci*. Similarly, the "diffraction" force on the i^{th} *column* segment in the (x_i, y_i, z_i) coordinate system can be obtained for the $j=2$ mode,

$$Y_{ci}^D e^{i\omega t}=(a_{22} \int v_{cyi} dz_i + b_{22} \int v_{cyi} dz_i)_{ci} \tag{58}$$

Similarly, for $j=1$ on the i^{th} hull and column segments, respectively, the "diffraction" force (54) becomes,

$$X_{hi}^D e^{i\omega t}=(a_{11} \int \dot{v}_{hxi} dx_i + b_{11} \int v_{hxi} dx_i)_{hi} \tag{59}$$

$$X_{ci}^D e_i^{\omega t}=(a_{11} \int \dot{v}_{cxi} dz_i + b_{11} \int v_{cxi} dz_i)_{ci} \tag{60}$$

For $j=3$ on the i^{th} hull and column segments, respectively, the "diffraction" force (54) becomes,

$$Z_{hi}^D e^{i\omega t}=(a_{33} \int \dot{v}_{hzi} dx_i + b_{33} \int v_{hzi} dx_i)_{hi} \tag{61}$$

$$Z_{ci}^D e^{i\omega t}=(a_{33} \int \dot{v}_{czi} dz_i + b_{33} \int v_{czi} dz_i) ci \tag{62}$$

For the "diffraction" forces (57) to (62), the integrals associated with the water-particle orbital accelerations, $\dot{v}_k$, are exactly the same as the corresponding integrals for the Froude-Krilov forces (37) and (38).

However, the Froude-Krilov forces (37) and (38) for example are associated with the displaced-mass of the segments, while the "diffraction" forces (57) and(58) are associated with the added mass:for example of Y_{hi}^{F-K} and $Y_{hi}^{D\dagger}$, which act on the i^{th} hull segment,

$$Y_{hi}^{F-K} e^{i\omega t}=-\frac{m_{hi}}{L_i} \int \dot{v}_{hyi} dx_i \tag{37}$$

and

$$Y_{hi}^D e^{i\omega t}=-\frac{\Delta m_{hyi}}{L_i} \int \dot{v}_{hyi} dx_i \tag{63}$$

where

$\frac{\Delta m_{hyi}}{L_i}=a_{22}$=added mass per unit hull length L_i the i^{th} segment in the y_i-direction (64)

It is reminded that the assumption to move the displaced mass outside the integral of the acceleration in (54) was used for the derivation of the Froude-Krilov forces (37) and (38). But the derivation of the "diffraction" force (57) to (62) uses the same assumption for keeping ϕ_I independent of the line integral (55).

The papers [1, 2, 4, 6, 11, 12] use the forms of the diffraction forces (57) to (62) without any preceding derivations which lead to these equations and without clearly relating (57) to (62) to the diffraction force. Again it is shown that potential flow theory approach lead the diffraction forces (52) to the forms (57) to (62). Of course, the form (52) is more general than the forms (57) to (62). The differences between the form (52) and the forms (57) to (62) of the diffraction forces are the consequent results due to the assumptions applied to get the forms (57) to (62).

The particle acceleration and the particle velocity are previously given by the equations (31) and (32), respectively. The integrals associated with the particle acceleration and particle velocity (57) to (62) are already evaluated for the Froude-Krilov forces (37) to (44).

Final forms of the diffraction forces acting on the displaced-mass center of the i^{th} column and hull segments at the points (x_{ci}, y_{ci}, z_i) in the x_i-, y_i-, and z_i-directions, respectively are summarized as in the following. Taking Re $[X_j^D e^{i\omega t}]$ gives

$$X_{ci}^D=\omega A Q_o(k)\cos\beta_i(\omega\Delta m_{cxi}\sin\tau_i+C_{xi}\cos\tau_i) \quad (65)$$

$$X_{hi}^D=\omega A\cos\beta_i[\omega\Delta m_{hxi}I_{si}(k)+H_{xi}I_{ci}(k)] \quad (66)$$

$$Y_{ci}^D=-\omega A Q_o(k)\sin\beta_i(\omega\Delta m_{cyi}\sin\tau_i+C_{yi}\cos\tau_i) \quad (67)$$

$$Y_{hi}^D=-\omega A\sin\beta_i[\omega\Delta m_{hyi}I_{si}(k)+H_{yi}I_{ci}(k)] \quad (68)$$

$$Z_{ci}^D=-\omega A P_o(k)(\omega\Delta m_{czi}\cos\tau_i-C_{zi}\sin\tau_i) \quad (69)$$

$$Z_{hi}^D=-\omega A[\omega\Delta m_{hzi}J_{ci}(k)]-H_{zi}J_{si}(k)] \quad (70)$$

where

$\frac{\Delta m_{czi}(\omega)}{H_i}=a_{11}$ for the i^{th} column (71)

$\frac{\Delta m_{hxi}(\omega)}{L_i}=a_{11}$ for the i^{th} hull (72)

$\frac{\Delta m_{cyi}(\omega)}{H_i}=a_{22}$ for the i^{th} column (73)

$\frac{\Delta m_{hyi}(\omega)}{L_i}=a_{22}$ for the i^{th} hull (74)

$\frac{\Delta m_{czi}(\omega)}{H_i}=a_{33}$ for the i^{th} column (75)

$\frac{\Delta m_{hzi}(\omega)}{L_i}=a_{33}$ for the i^{th} hull (76)

C_{xi}, C_{yi}, C_{zi}=dampings on the i^{th} column in the x_i-, y_i-, and z_i-directions, respectively as defined by the equation(114) (77)

H_{xi}, H_{yi}, H_{zi}=dampings on the i^{th} hull in the x_i-, y_i-, and z_i-directions, respectively as defined by the equation(115) (78)

The rest of the notations is previously defined by the relationships (45) to (49).

3.4. Motion-Dependent Force

The segments of the rig members undergo rigid-body, oscillatory motion for the rig under motion; and the segment motions induce the motion-dependent forces. The forces due to the rig motion are obtined as though the rig (more specially, the member segments) undergoes an oscillatory motion in still water. We shall derive the motion-dependent force in the segment coordinate system.

The "motion-dependent" forces (27) with the body boundy condition (18) on i^{th} segment in the segment (x_i, y_i, z_i) coordinate is

$$X_j^M e^{i\omega t}=-i\rho\omega\iint_{s_i} n_j\sum_{k=1}^{3}x_k\phi_k ds_i \quad (79)$$

$$X_j^M e^{i\omega t}=\sum_{k=1}^{3}\int t_{jk}x_k dx_L$$

where t_{jk} are defined by the equation (55), and x_k are the motions of the i^{th} segment at the point (x_{ci}, y_{ci}, z_i).

Applying the equation (55), the "motion-dependent" forces (79) can be divided into the force due to the acceleration and velocity of the i^{th} hull segment,

$$X_{hi}^M e^{i\omega t}=\sum_{k=1}^{3}\int_{-Li/2}^{Li/2}(\omega^2 a_{jk}-i\omega b_{jk})x_k dx_i$$

$$=-\sum_{k=1}^{3}(\ddot{x}_k\int_{L_i}a_{jk}dx_i+\dot{x}_k\int_{L_i}b_{jk}dx_i \quad (80)$$

where $\ddot{x}_k$ is the acceleration of the i^{th} segment, and $\dot{x}_k$ is the velocity of the i^{th} segment.

X_k are defined by the equations (1) to (3) for $k=1,2,3$ directions for the i^{th} hull X_2 is defined

$$\eta_{hi}=\eta+x_{ci}\psi+z_{hi}\phi)\cos\gamma_i -(\xi-z_{hi}\theta-y_{ci}\psi)\sin\gamma_i \quad (81)$$

Since $a_{12}=a_{13}=a_{23}=0$ and $b_{12}=b_{13}=b_{23}=0$ for the i^{th} cylinder segment, the "motion-dependent" force (80) on the i^{th} column and hull segments can be written, taking $R_e[X_j^M e^{i\omega t}]$, for $j=1$ on the i^{th} column and hull, respectively,

$$X_{ci}^M=-H_i(a_1\ddot{\xi}_{1ci}+b_{11}\dot{\xi}_{ci})_{ci} \quad (82)$$

$$X_{hi}^M=-L_i(a_{11}\ddot{\xi}_{hi}+b_{11}\dot{\xi}_{hi})_{hi} \quad (83)$$

for $j=2$ on the i^{th} column and hull, respectively,

$$Y_{ci}^M=-H_i(a_{22}\ddot{\eta}_{ci}+b_{22}\dot{\eta}_{ci})_{ci} \quad (84)$$

$$Y_{hi}^M=-L_i(a_{22}\ddot{\eta}_{hi}+b_{22}\dot{\eta}_{hi})_{hi} \quad (85)$$

for $j=3$ on the i^{th} column and hull, respectively,

$$Z_{ci}^M=-H_i(a_{33}\ddot{\zeta}_{ci}+b_{33}\dot{\zeta}_{ci})_{ci} \quad (86)$$

$$Z_{hi}^M=-L_i(a_{33}\ddot{\zeta}_{hi}+b_{33}\dot{\zeta}_{hi})_{hi} \quad (87)$$

The motion-dependent force equations (82) to (87) are the same as the equation forms used by the others [1, 3, 4, 6, 11, 12]. For the derivation of the motion-dependent force equations (82) to (87), the only assumption applied is that the cross section of the segment does not vary along the segment axis. This assumption was already applied to get the equation (27) and is not additional assumption. Also the assumptions made for the Froude-Krilov forces (37) and (38) and diffraction forces (57) to (62) are not necessary for the derivation of the motion-dependent force equation (80).

So far, the equations for the Froude-Krilov force including the hydrostatic force, the diffraction force, and the motion-dependent force have been derived and discussed strictly in the segment (x_i,y_i,z_i) coordinate system for the i^{th} member segments of the floating rig or structure. In the next these force equations derived in the segment (x_i,y_i,z_i) coordinate systems will be transformed to the force equations in the body (x,y,z) coordinate system for the entire floating structure.

3.5. Total Forces on the Floating Structure

Total forces acting on the entire structure or rig in the body (x,y,z) coordinate system can be obtained in terms of the total forces (24) which are separately derived in the segment (x_i,y_i,z_i) coordinate system for the individual column and hull segments as follows. The directions of the total forces (24) in the segment coordinate system are oriented toward the x-, y-, and z-directions of the body coordinate system and then are summed in the body (x,y,z) coordinate system for all the submerged portions of the column and hull segments.

Thus the above sums of the total forces (24) give the total forces in the body (x,y,z) coordinate system on the submerged portion of the entire floating structure,

$$X=\sum_i^N X_i'=\sum_{i=1}^N[(X_{ci}+X_{hi})\cos\gamma_i -(Y_{ci}+Y_{hi})\sin\gamma_i] \quad (88)$$

$$Y=\sum_i^N Y_i'=\sum_{i=1}^N[(Y_{ci}+Y_{hi})\cos\gamma_i +(X_{ci}+X_{hi})\sin\gamma_i] \quad (89)$$

and

$$Z=\sum_i^N Z_i'=\sum_{i=1}^N(Z_{ci}+Z_{hi}) \quad (90)$$

where N is the total number of pairs of the column and hull segments. The directions of the total forces (88), (89), and (90) are in the x-, y-, and z-directions.

3.5.1. Special Cases

When all the hull segments are parallel to each other, or $\gamma_i=0$, the second terms of equations (88) and (89) vanish, since $\sin\gamma_i=0$. Then for $\gamma_i=0$, equations of the total forces become similar for the case of infinite depth to the force equations of Kim [8] and Ochi [11].

Furthermore, when $\gamma_i=0$ and $y_{ci}=0$, then the equations of the total forces can be applied to the case of a monohull structure, submerged below or in the free surface.

3.6. Total-Force Distributions Along the Structural Members

The total forces (24) in the segment (x_i,y_i,z_i) coordinate on the individual column- and hull-member segments can be used as the total force distributions

along the column members and hull members. Details of equation (24) are presented in equations (39) to (44), (65) to (70), and (82) to (87). For fine distributions of the total forces along the members, the total force computations can be made for as many segments for the given structural members as desired within the framework of the theory and assumptions involved. The total force distributions along the structural members in the segment coordinate are essential information for the structural analysis of a floating rig or structure. With an increase in the number of the member segments, finer total force distributions along the structure or rig members can be obtained. For the structural analysis additional inputs of current force, mooring line effects, and wind forces should be included.

On the other hand, the total forces (88) to (90) in the body (x,y,z) coordinate system on the entire submerged portion of the structure can be used for the equations of motion. From the equations of motion with the total forces (88) to (90), the added mass coefficients, A_{jk}, the damping coefficients, B_{jk}, the hydrostatic coefficients, C_{jk}, and the exciting force and moments, F_j will be derived. These coefficients and exciting force and moments are defined in the body coordinate system.

4. The Coefficients and the Exciting Forces and Moments

4.1. The Equations of Motion

The linearized equations of motion in the body (x, y, z) coordinate system for a floating structure are as follows:

$$M\xi = X \tag{91}$$

$$M\eta = Y \tag{92}$$

$$M\zeta = Z \tag{93}$$

$$I_x\ddot{\phi} = \sum_{i=1}^{N}\left[-\int_{H_i}\left(\frac{d}{dz}Y'_{ci}\right)z\,dz + Y'_{hi}z_{hi} + z_i y_{ci} + g(m_{hi}z_{hi} - m_{ci}z_1)\phi\right] \tag{94}$$

$$I_y\ddot{\theta} = \sum_{i=1}^{N}\left[\int_{H_i}\left(\frac{d}{dz}X'_{ci}\right)z\,dz - X'_{hi}z_{hi} - Z'_i x_{ci} - \int_{L_i}\left(\frac{d}{dx}Z_{hi}\right)x\,dx + g(m_{hi}z_{hi} - m_{ci}z_1)\theta\right] \tag{95}$$

$$I_z\ddot{\psi} = \sum_{i=1}^{N}\left[-X'_i y_{ci} + Y'_{ci}x_{ci} + \int_{L_i}\left(\frac{d}{dx}Y'_{hi}\right)x\,dx\right] \tag{96}$$

where

$$X'_{hi} = X_{hi}\cos\gamma_i - Y_{hi}\sin\gamma_i$$

$$X'_{ci} = X_{ci}\cos\gamma_i - Y_{ci}\sin\gamma_i$$

$$Y'_{ci} = Y_{ci}\cos\gamma_i + X_{ci}\sin\gamma_i$$

$$Y'_{hi} = Y_{hi}\cos\gamma_i + X_{hi}\sin\gamma_i$$

$$z_1 = \frac{1}{H_i}\int_{-(H_i+b)}^{-b} z_i\,dz_i$$

I_x, I_y, I_z are the mass moments of inertia about the x-, y-, and z-axis, respectively.

It is noted that the vertical forces Z in (93) and Z_i in (94) and (95) also contain the hydrostatic restoring forces for the motions $\zeta_i(t)$ (heave, roll, and pitch) with the waterplane area: these hydrostatic restoring forces are included in the Froude-Krilov forces (41) and (44). It is also noted that the hydrostatic buoyancy moments now appear in the roll and pitch equations, (94) and (95).

4.2. The Coefficients and the Exciting Forces and Moments in the Body Coordinate

The added mass coefficients, a'_{jk}, the damping coefficients, b'_{jk}, the hydrostatic restoring force coefficients, c'_{jk}, and the exciting forces and moments, f'_j, can be obtained in the body (x, y, z) coordinate system for the individual segments as follows: $j,k=1,2,...6$. Substituting the total forces (88) to (90) derived for the body coordinate system into the equations of motion (91) to (96) and grouping all the resulting terms in $\ddot{x}_j, \dot{x}_j$, and x_j $(j=1,2,...6)$ before performing the summations give $a'_{jk}, b'_{jk}, c'_{jk}$, and f'_j in the body coordinate system for the individual segments; $j,k=1,2,...6$.

The $a'_{jk}, b'_{jk}, c'_{jk}$, and f'_j in the body coordinate system are the segmental (two dimensional) values, a_{jk}, b_{jk} (55), c_{jk}, and $f_j, j,k=1,2,3$ in the segment (x_i, y_i, z_i) coordinate system oriented to the body coordinate system, and additionally include coupling coefficients $(j,k=4,5,6)$ and exciting moments $(j=4,5,6)$. It is noted that for both the body and segment coordinate systems, $c'_{jk}=c_{jk}$, and also for $j=1,2,3$, $a'_{jj}=a_{jj}$ and $b'_{jj}=b_{jj}$. For the monohull including ships ($\gamma_i=0$ and $y_{ci}=0$) and the multihull structure whose hull segments are parallel to each other ($\gamma_i=0$),

we get the relationship $a'_{jk}=a_{jk}$, $b'_{jk}=b_{jk}$, and $f'_j=f_j$ for the individual segments and $j,k=1,2,3$. On the other hand, for multihull structures whose hull segments are not parallel to each other ($\gamma_i\neq 0$), we can additionally have nonzero values of a'_{jk} and b'_{jk} (55) and consequently of A_{jk} and B_{jk}, (7) and (8), as compared to the equations of ship motion or the case of $\gamma_i=0$ and $y_{ci}=0$.

Summations of the above a'_{jk}, b'_{jk}, c_{jk}, and f'_j, respectively for the total number of the segments, N in the body coordinate system give the coefficients and the exciting forces and moments for the entire body as follows,

$$A_{jk}=\sum_{i=1}^{N} a'_{jk} \tag{97}$$

$$B_{jk}=\sum_{i=1}^{N} b'_{jk} \tag{98}$$

$$C_{jk}=\sum_{i=1}^{N} c_{jk} \tag{99}$$

and

$$F_j=\sum_{i=1}^{N} f'_j=X'^{F-K}_j+X'^{D}_j, \tag{100}$$

$j,k=1,2\cdots 6$.

The exciting forces (100) are derived above $j=1,2,3$ in detail with the Froude-Krilov forces (39) to (44) and the "diffraction" forces (65) to (70). Since A_{jk}, B_{jk}, and C_{jk} in the body coordinate system can be expressed in terms of a_{jk}, b_{ik}, and c_{jk} which are the values for the individual i^{th} segments in the segment coordinate system, the coefficients for the segments in the (x_i, y_i, z_i) coordinate system are further discussed later in details.

4.3. The Resulting Assumptions on the Hydrodynamic Coefficients and the Exciting Forces and Moments

In the total force equations (88) to (90) the total forces on the individual column and hull segments are summed in the body coordinate system. Among the total force components, the diffraction forces (65) to (70) and the motion-dependent forces (82) to (87) are shown to be expressed in terms of a_{jj} and b_{jj} which are cylindrical segmental values of the added mass and damping coefficients in the segment coordinate. Therefore for the total force equations (88) to (90) the added mass and damping for the diffraction force and the motion-dependent force on the i^{th} column segment are added to those for the correponding i^{th} hull segment.

This simple summation of the added mass and damping in the above for a pair of the i^{th} column and hull segments assumes that the possible hydrodynamic interference effect at the joint of the column and hull is small and ignored. Also the simple addition of the total forces on the i^{th} segments implies that the possible hydrodynamic interferences between the hull segments or the column segments are ignored. For the majority of the existing semi-submersible-like floating structures, the distance between the hulls or columns are so far that the hydrodynamic interferences between them can safely be ignored for those structures. When there are significant hydrodynamic interferences at the joint of the column and hull and between the columns or hulls, those interferences can be taken into account by the proper added mass and damping for the numerical computations of the motions and forces. Also the hydrodynamical end effect of the segments, if significant, can be treated similarly as above.

4.4. Hydrostatic Restoring Coefficients

The hydrostatic restoring coefficients C_{jk} are obtained previously from the equations of heave (93), roll (94) and pitch (95) for the (x,y,z) coordinate system,

$$C_{33}=\rho g\sum_{i=1}^{N} A_{wpi} \tag{101}$$

$$C_{31}=C_{43}=\rho g\sum_{i=1}^{N} y_{ci}A_{wpi} \tag{102}$$

$$C_{53}=C_{35}=-\rho g\sum_{i=1}^{N} x_{ci}A_{wpi} \tag{103}$$

$$C_{51}=C_{45}=-\rho g\sum_{i=1}^{N} x_{ci}y_{ci}A_{wpi} \tag{104}$$

$$C_{44}=g\sum_{i=1}^{N}(\rho y^2_{ci}A_{wpi}+m_{ci}z_1-m_{hi}z_{hi}) \tag{105}$$

$$C_{55}=g\sum_{i=1}^{N}(\rho A_{cpi}x^2_{ci}+m_{ci}z_1-m_{hi}z_{hi}) \tag{106}$$

where

$$A_{wpi}=A_{cwi}+A_{hwi} \tag{107}$$

$$z_1=\frac{1}{H_i}\int_{-(H_i+b)}^{-b} z_i dz_i \tag{108}$$

z_{hi}=mean vertical distance of the i^{th} hull segment below the rig CG

The C_{jk} are independent of wave frequency and forward speed. The last two restoring coefficients can also be expressed in terms of metacentric heights

$$C_{44}=\rho g V z_\phi,\ C_{55}=\rho g V z_\theta \tag{109}$$

where

$V=\sum_{i=1}^{N} V_i$=displaced volume of the entire structure

z_ϕ=transverse metacentric height

z_θ=longitudinal metacentric height.

For the reasons described previously, $A_{hwi}=0$ for the majority of the semisubmersible drilling rigs for the drilling operational mode.

For a floating rig with a lateral symmetry about the x-z plane, $C_{34}=C_{43}=0$[8, 11, 12, 14, 15]. For a floating rig with both the lateral symmetry about the x-z plane and the fore-and-aft symmetry about the y-z plane, $C_{34}=C_{43}=C_{35}=C_{53}=C_{45}=C_{54}=0$.

4.5. Added Mass and Damping Coefficients in the Segment Coordinate

There has been no available theoretical method of accurately computing the hydrodynamic (added mass and wave damping) coefficients of the floating rig members including the possible hydrodynamic interferences at the joints of the (vertical) column and (horizontal) hull segments (Fig. 1-a) and of the oval footing with a column (Fig. 1-b) Viscous damping will be separately discussed later. The papers [1, 3, 6, 8, 11, 12] have separately treated the column and hull segments (e.g. MOHOLE and Ocean Traveller series) as if the segments are twe-dimensional, or with no hydrodynamic interferences at the joints. But a Physical intuition is that the joint produces (threedimensional) hydrodynamic interference which would be more complex under the effects of the free surface and water depth. Also the oval footing with a vertical colum (e.g. SEDCO 135 series and Pentagone 80 and 90 series) produces the three-dimensional flow phenomena for the three-dimensional oval footing itself and also at the joint of the oval footing with a column: for this model, perpaps the method [21] may be used to calculate the heave coefficients. The same argument can apply to many other types of the rig members.

Also very few experimental, hydrodynamic coefficient data have been published for the submerged segments under the influence of the free surface or water depth or both.

4.5.1. Added Mass and Wave Damping

However, there have been a few methods of theoretically computing the two-dimensional added mass and wave damping, and we shall here limit to Frank's method [5] and limited experimental data [4] for the case of MOHOLE drilling rig used for the present motion computations. Although the Frank's method is generally accurate for the two-dimensional body in the free surface [15], the present author's first-hand information on some unpublished experimental data shows that some reservation should be made for a submerged two-dimensional body oscillating very close to the free surface:this subject will not be discussed any further in this paper. For the case of SEDCO 135-F drilling rig, actual hydrodynamic coefficients measured by the planar motion mechanism test [4] are used for the computations of the motions. For some other shapes of the submerged segments, St. Dennis [15] made a literature survey. Also for some submerged bodies without the free-surface effect, Wendel [19] lists the added mass coefficients. Before defining the hydrodynamic coefficients, it is noted that rational comparison of the computations of the total forces and motion by the potential flow approach (24) and by the approach of equations (36), (54), and (80) can not be made unless the accurate values of the hydrodynamic coefficients are used. All discussions in this section are made in the segment (x_i, y_i, z_i) coordinate system.

The added mass on the i^{th} segments in the x_i-, y_i-, and z_i-directions, respectively are defined as (also refer to equations (71) to (76)) in terms of the corresponding added mass coefficients,

$$a_{jj}(\omega)H_i=\Delta m_{cji}(\omega)=m_{ci}\mu_{cji}(\omega) \tag{110}$$

for the column segment, and

$$a_{jj}(\omega)L_i=\Delta m_{hji}(\omega)=m_{hi}\mu_{hji}(\omega) \tag{111}$$

for the hull segment. μ_{cji} are the added mass coefficients for the i^{th} column segment for the j^{th} mode of oscillation in the segment (x_j, y_j, z_i) coordinate system. μ_{hji} are the added mass coefficients for the i^{th} hull segment for the j^{th} mode of oscillation. The added masses per unit length, $a_{jj}(j=1, 2, 3)$ are defined by the relationships (71) to (76) which do not clearly

distinguish in notations for the column and hull, but are appropriately distinguished whenever they appear.

The added mass coefficients on the i^{th} segments are defined as,

$$\mu_{cji}(\omega)=\frac{(in\text{-}phase\ force)ji}{m_{ci}\omega^2\bar{A}}=\frac{\Delta m_{cji}(\omega)}{m_{ci}} \tag{112}$$

for the column and

$$\mu_{hji}(\omega)=\frac{(in\text{-}phase\ force)ji}{m_{hi}\omega^2\bar{A}}=\frac{\Delta m_{hji}(\omega)}{m_{hi}} \tag{113}$$

for the hull. j indicates the modes of the i^{th} segment oscillations (j=1, 2, 3); x_i for $j=1$, y_i for $j=2$, and z_i for $j=3$. $\bar{A}$ is the oscillation amplitude.

The damping on the segments consists of the wave damping and linearized viscous damping. The linearized viscous damping and the wave damping on the i^{th} segment for the j^{th} modes of oscillation are defined in terms of the respective damping coefficients,

$$C_{ji}=\frac{8}{3\pi}C_d\frac{\rho}{2}S_{ci}\left|v^r_{cji}\right|+\lambda_{cji}(\omega)m_{ci}\omega A \tag{114}$$

for the column, and

$$H_{ji}=\frac{8}{3\pi}C_d\frac{\rho}{2}S_{hi}\left|v^r_{hji}\right|+\lambda_{hji}(\omega)m_{hi}\omega A \tag{115}$$

for the hull, where

C_d=drag coefficient on the segment obtained, without the factor $8/3\pi$, for Reynolds number R_e.

S_{ci}=principal projected area of the column segment

S_{hi}=principal projected area of the hull segment

v^r_{cji}=relative column velocity for the j^{th} mode of motion, and is defined later.

v^r_{hji}=relative hull velocity for the j^{th} mode of motion, and is defined later

$\lambda_{cji}(\omega)$=wave-damping coefficient for the i^{th} column for the j^{th} mode of oscillation

$\lambda_{hji}(\omega)$=wave-damping coefficient for the i^{th} hull for the j^{th} mode of oscillation

The first terms of the dampings (114) and (115) are viscous damping components, and the second terms are wave-damping components. The dampings (114) and (115) can significantly affect the motions of a floating structure near the resonance frequency. Due to the differences in the damping characteristics, the viscous damping are discussed later, following the discussion on the added mass and wave damping.

The wave-damping coefficients on the i^{th} segment for the j^{th} mode of oscillation are difined as

$$\lambda_{cji}(\omega)=\frac{(\text{out-of-phase force})_{ji}}{m_{ci}\omega^2\bar{A}} \tag{116}$$

for the column, and

$$\lambda_{hji}(\omega)=\frac{(\text{out-of-phase force})_{ji}}{m_{hi}\omega\bar{A}^2} \tag{117}$$

The wave damping coefficients can also be expressed as

$$b_{jj}(\omega)H_i=\lambda_{cji}(\omega) \tag{118}$$

for the column segment, and

$$b_{jj}(\omega)\ L_i=\lambda_{hji}(\omega) \tag{119}$$

for the hull segment. b_{ii} in equations (118) and (119) contain wave-damping component only.

The added mass and the wave damping of a *hull* (horizontal) segment immersed below the free surface are a function of

- Frequency of oscillation
- Immersed depth below the free surface
- Direction of oscillation
- Cross-sectional geometry
- Water depth

The normalized oscillation frequency range of practical interest can be from $\omega=0.25$ to 1.0 (or roughly 5 to 25 seconds wave period): $\bar{\omega}=\omega^2 a/g$ where ω is the oscillation frequency in rad/sec and is the same as the wave frequency, a is the segment's cross-

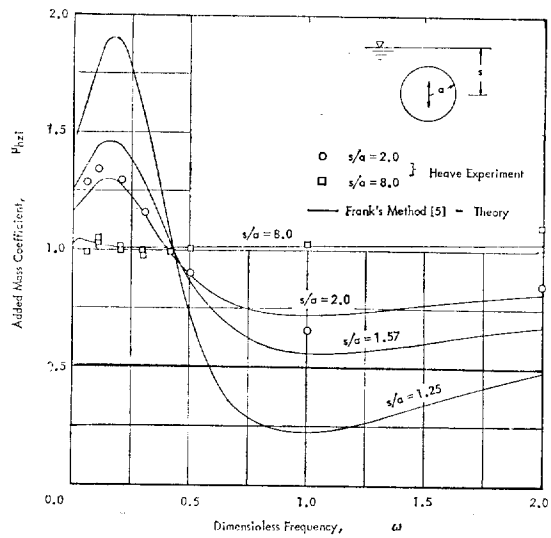

Fig. 4-a. Added-Mass Coefficients for a Horizontal Circular Cylinder Below a Free Surface(infinite depth).

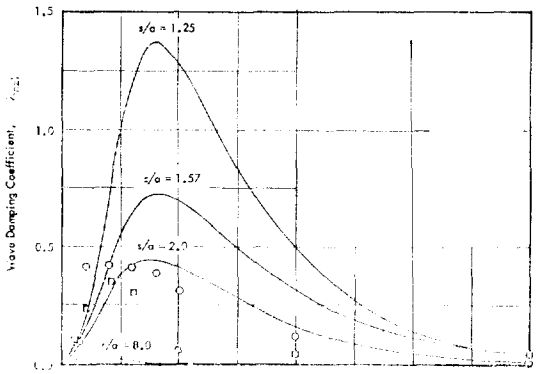

Fig. 4-b. Wave-Damping Coefficients for a Horizontal Circular Cylinder Below a Free Surface (infinite depth).

sectional dimension. This frequency range is usually adequate to describe the frequency range of interest for the main column and hull segment sizes of the majority of the floating, multihull structures including semisubmersible drilling rigs in the ocean. At both very low and high frequencies, the wave damping vanishes (Fig. 4-b). Also at the higher frequency range the added mass becomes independent of the oscillation frequency and becomes constants for given values of the other parameters (Fig. 4-a) In an infinite fluid, the coefficients are independent of the oscillation frequency.

As the immersion depth, s , becomes shallower or gets closer to the free surface, the free-surface effect gets stronger over the frequency range: the maximum added mass coefficient gets larger, the minimum value gets smaller, and the maximum wave-damping coefficient gets larger. The immersion ratio, defined as s/a for the main, circular and square or similar cross-sectional, hull segments of the semisubmersible drilling rigs are $s/a \lesssim 2$ for either towing mode or transient operational draft and are $s/a \geq 2 \sim 3$ for drilling operational draft. Further discussion for two geometrics of semisubmersible drilling rigs are made later.

In an infinite fluid, the coefficients are the same for a two-dimensional symmetric body for the different transverse directions and all frequencies of oscillations. For small values of s/a ratio or when the hull segments are close to the free surface, the added mass and damping coefficients can be different for the different directions of oscillations. Also for the segments of different cross-sectional geometries the added-mass coefficients and the wave-damping (also the viscous damping) coefficients are different.

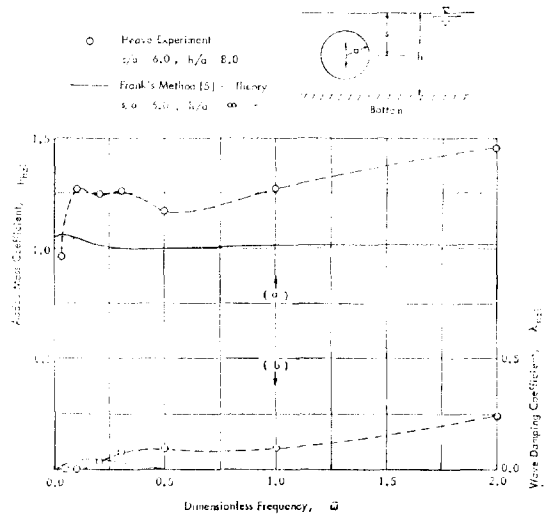

Fig. 5-a. Added-Mass Coefficients for a Horizontal Circular Cylinder Below a Free Surface (finite depth).

Fig. 5-b. Wave-Damping Coefficients for a Horizontal Circular Cylinder Below a Free Surface (finite depth).

For a finite-depth water with a free surface, the added mass coefficients and the wave damping coefficients in general (Figs. 5-1 and 5-b) get larger over the frequency range of interest and also with an increase of the higher frequency, as compared to the case of infinite fluid bounded by a free surface only. It is noted that to the author's knowledge there have been available in the published literature no theoretical computations of the added mass and wave damping for a completely immersed, oscillating body under the influence of the water depth or under the influence of both the water depth and the free surface. In the next we shall discuss experimentally-validated values [4] of the added mass coefficients and wave damping coefficients for two different segments commonly used as member segment of the semisubmersible drilling rigs.

Circular Cylinder. Floating structure such as MOHOLE drilling rig consists of many segments of circular cross section (Fig. 1-a). The possible hydrodynamic interferences at the joint of two or more members and the hydrodynamic end effect are ignored for

the present discussion of the added mass and wave damping of a circular cylinder in the segment coordinate system.

For a (horizontal) *hull* segment, $\mu_{hxi}\approx 0$ and $\mu_{hyi}\approx\mu_{hzi}$, and also $\lambda_{hxi}\approx 0$ and $\lambda_{hyi}\approx\lambda_{hzi}$. Consequently, the x_i-directional component of the diffraction force (66) and the motion-dependent force on the i^{th} hull (83) vanish, $X_{hi}^{D}=0=X_{hi}^{M}$. For a surface-piercing (vertical) *column* segment, $\mu_{czi}\approx 0$ and $\mu_{cxi}=\mu_{cyi}$, and also $\lambda_{czi}\approx 0$ and $\lambda_{cxi}=\lambda_{cyi}$. Consequently, the x_i -directional component of the diffraction force (69) and the motion-dependent force (86) on the i^{th} column vanish, or $Z_{ci}^{D}=0=Z_{ci}^{H}$.

For a surface-piercing vertical circular cylinder (*column*) $\mu_{cxi}=\mu_{cyi}\approx 1$, [18] if the diameter of the cylinder is small compared with its length. This is partially supported by an experimental result obtained for a model of submerged oval footing with a vertical, surface-piercing cylinder (Fig. 6-a) which is discussed later. In Fig. 6-a, μ_{xi} and μ_{yi} are practically independent of the oscillation frequency for $s/a=8.0$ ($H_i/r=6.0$) and $h/a=\infty$: this result can indirectly indicate that for the surface-piercing, vertical circular cylinder μ_{cxi} and μ_{cyi} are constant for $s/a\geq 8.0$ ($H_i/r\geq 6.0$) and $h/a=\infty$. Figure 6-b shows that the wave damping is small: r is the radius of the column.

For *infinite depth*, Figures 4-a and 4-b show the heave added-mass coefficients and wave-damping coefficients which are both theoretically [5] and experimentally [4] determined for a completely immersed model of a horizontal, two-dimensional circular cylinder in infinitely deep water (40 times the radius of the cylinder in the experiment) with a free surface. The experimental data are obtained with the planar motion mechanism [4]. The wave-damping coefficients for $s/a=2.0$ are obtained by subtracting the total (or viscous) damping coefficients obtained for $s/a=8.0$ and $h/a=\infty$ from total damping coefficients obtained for $s/a=2.0$. The measured viscous damping coefficients for $s/a=8.0$ and $h/a=\infty$ are small and nearly a constant. Comparison of the theoretical calculation [5] with limited experimental points [4] for the immersion depth ratio $s/a=2.0$ shows a good agreement except for the wave damping. The frequency for the maximum wave damping obtained by the experiment is lower than the frequency for the maximum wave damping obtained by the teoretical method.

For *finite depth*, the added mass coefficients are larger over the frequency range as compared to the infinite water depth. Finite depth ratio is defined as h/a where h is the water depth. Theoretical basis of the Reference [5] indicates that the added mass and damping computations by the method [5] for $h/a=\infty$ would be more accurate for $s/a>2.0$ than for $s/a=2.0$. For $s/a=2.0$ and $h/a=\infty$ the computed added-mass coefficients are validated by the experiment(Fig. 4-a). So the conjecture is that the added-mass computations (Fig. 5-a) by the method [5] for $s/a=6.0$ and $h/a=\infty$ are accurate. Figure 5-a compares the expeximentally determined heave added-mass coefficients for $s/a=6.0$ and $h/a=8.0$ with the computed heave values for $s/a=6.0$ and $h/a=\infty$. Comparison shows that, when compared with the computed values for infinite depth, the experimentally-determined added-mass coefficients for finite depth are larger over the frequency range except at $\bar{\omega}<0.1$, that as the frequency gets higher, the experimental values for finite depth get larger, and that for $\bar{\omega}<0.1$ the experimental value for finite depth gets smaller. The wave damping coefficients for $s/a=6.0$ and $h/a=8.0$ are small(Fig. 5-b) but shows a trend that the coefficients increases as the frequency increases beyond a certain value.

Also an experimental-data curve for the immersion depth ratio $s/a\geq 6.0$ for finite depth [4] (Figs. 5-a and 5-b) show that the free surface effect on or the frequency dependence of the coefficients practically vanishes for the heave oscillation. The author's first-hand information is that the planar motion mechanism test of the present circular cylinder showed little difference between the measured coefficients for the $s/a=2.0$, $h/a=8.0$ and the $s/a=2.0$, $h/a=\infty$,

In design and operational practice the immersion depth ratio is $s/a=2.5\sim 3$ for the drilling draft of many semisubmersible rigs such as the MOHOLE rig with circular cylindrical hulls and $s/a=1.5\sim 2.0$ for the survival draft. Usually the survival draft is shallower than the operational drilling draft, since the adequate clearance between the instant wave surface and the lower side of deck should be ensured for the

safety of the rig in rough seas. For the MOHOLE rig, the drilling draft ranges from 60 ft (18.29m) to 70 ft (21.34m) corresponding to $s/a=2.43\sim3.0$, and the survival draft is 45 ft (13.72m) corresponding to $s/a=1.57$. The water depth for the present calculation is $h=200$ ft (60.96m) which corresponds to the water depth to hull radius ratio of $h/a=11.43$ and for the 70 ft draft $s/a=3.0$. For these values of h/a and s/a, the water depth effect on the coefficients is ignored on the basis of the experimental evidence described above, and only the free surface effects are considered in the calculations of the added mass and wave damping coefficients. Notice that the variation of the coefficients due to the free-surface effect is the greatest within the frequency range of practical interest.

Oval Footing With a Circular Cylinder. Floating structure such as the SEDCO 135 series and Pentagon 80 and 90 series consists of several oval footings each with a vertical cylinder (Fig. 1-b) for which the added mass coefficients and wave damping coefficients are three dimensional. For the surface piercing, long (vertical) column segment ignoring the hydrodynamic interferences at its joint with the oval footing, $\mu_{czi}=0$ and also $\lambda_{czi}=0$.

Figures 6-a and 6-b show the added-mass coefficients and wave-damping coefficients, respectively for a model of a submerged oval footing a vertical circular cylinder [4] which is a three-dimensional model. These coefficients are experimentally determined with the planar motion mechanism, as described above, for both infinite and finite water depths. The added-mass coefficients are expressed as $\mu_{yi}=\mu_{cyi}+\mu_{hyi}$ and $\mu_{zi}=\mu_{czi}+\mu_{hzi}$, and the corresponding wave-damping coefficients are expressed as $\lambda_{yi}=\lambda_{cyi}+\lambda_{hyi}$ and $\lambda_{zi}=\lambda_{czi}+\lambda_{hzi}$: here $\mu_{xi}=\mu_{yi}$ and $\lambda_{xi}=\lambda_{yi}$. These coefficients include the three-dimensional effect of the footing and the hydrodynamic-interference effect at the joint of the footing with the column.

In Figs. 6-a and 6-b, the immersion depth ratios (s/a) tested were different between $h/a=8.0$ and $h/a=\infty$. But the careful examination of the test data (Fig. 6-a) indicates the followings. For the $s/a=6.0$ and $h/a=8.0$, the free surface effect on the added mass coefficients, though small, appear at the lower frequency range for the vertical oscillations, but is

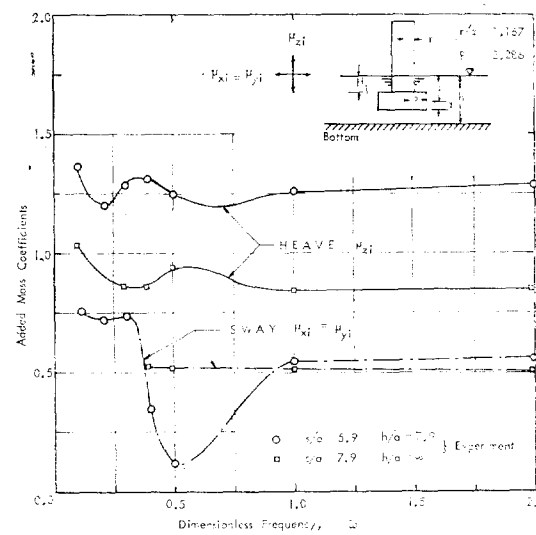

Fig. 6-a. Added-Mass Coefficients for a Model of Submerged Oval with Surface Piercing Vertical Circular Cyinder (infinite depth and finite depth).

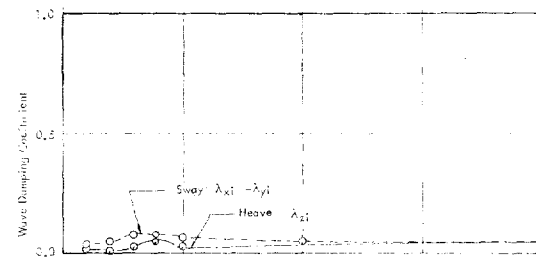

Fig. 6-b. Wave-Damping Coefficients for a Model of Submerged Oval with Surface-Piercing Vertical Circular Cylinder (infinite depth and finite depth).

significantly large for the horizontal oscillations. For the $s/a=8.0$ and $h/a=\infty$, the vertical coefficients, μ_{zi} are slightly influenced by at the lower frequency range by the free-surface effect, and the horizontal coefficients, μ_{xi} or μ_{yi} are practically independent of the free-surface effect or are independent of the oscillation frequency. The vertical coefficients μ_{zi} are larger over the frequency range for the finite depth, $h/a=8.0$ than for the infinite depth. The horizontal coefficients, μ_{xi} or μ_{yi} are only slightly larger at the higher frequency range for the finite depth than for the infinite depth. Also in general the closer to the bottom the model oscillates at the higher frequencies, the larger both the vertical and horizontal coefficients

become.

Figure 6-b shows that the wave-damping coefficients are negligibly small for both the vertical and horizontal oscillations. The wave damping coefficients are obtained by the same procedure as for the circular cylinder.

For the present heave calculations of the SEDCO 135-F rig, the 80-ft drilling draft corresponds to $s/a=5.4$, and the 120-ft water depth corresponds to $h/a=8.0$. The motion computations use the added mass coefficients and damping coefficients as shown in Figs. 6-a and 6-b. The footing of the SEDCO 135-F is slightly different from the present oval footing, but is very close in the hydrodynamic characteristics to it.

4.5.2. Viscous Damping

The viscous-damping components of the equations (114) and (115) are linearized with the factor 8/3, according to a method [2]. The relative velocities(114) and (115) are defined as the mean value of the oscillatory velocity of the i^{th} segments oscillatory motion relative to the water-particle oscillatory velocity at the i^{th} segment point (x_{ci},y_{ci},z_i) in the (x_i,y_i,z_i) coordinate system, or

$$v_{cji}^r=\frac{1}{H_i}\int_{-(H_i+b)}^{-b}(v_{cji}-\dot{x}_{cji})dz_i \tag{118}$$

for the column and j-directions, and for the i^{th} hull,

$$v_{hji}^r=\frac{1}{L_i}\int_{-L_i/2}^{L_i/2}(v_{hji}-\dot{x}_{hji})dx_i \tag{119}$$

Oscillatory motions of the i^{th} segment are defined by the relationships (1), (2), (3) and (81).

On the basis of the (oscillatory) relative velocity (118) and (119), Reynolds number is introduced as,

$$R_e=\frac{l|v_{cji}^r|}{\nu} \tag{120}$$

for the i^{th} column in the j-direction, and for the i^{th} hull,

$$R_e=\frac{l|v_{hji}^r|}{\nu} \tag{121}$$

where

l=characteristic length of the i^{th} segment normal to the direction of the oscillation

ν=kinematic viscosity.

For the Reynolds number defined above, the drag coefficient C_d can be obtained. The C_d does not depend on the free surface effect. The free surface effect on the damping is described above for the wave damping.

The j-directional oscillatory velocities of the i^{th} segment $\dot{x}_{ji}$, are initially unknown for the viscous damping force computations. For the present computations, $\dot{x}_{ji}$ are determined through an iteration process of the motion computations for given values of C_d. Initially the motion computations use $v_{cji}^r=v_{cji}, v_{hji}^r=v_{hji}$ with $\dot{x}_{cji}=0=\dot{x}_{hji}$ for given values of C_d, in the second time use $\dot{x}_{cji}$ and $\dot{x}_{hji}$ computed by the initial computation, and the iteration process continues until the computed motions converge to the respective final values. The damping force affects the motions near the respective modes of the motion-resonance frequencies only.

The value of C_d is determined empirically as $C_d=1.0$, when the computed resonance motion best fits the experimentally measured motions for both the MOHOLE rig and SEDCO 135-F rig. The interferences at the joints of the member segments, end effects and the interferences between the segments make it difficult to initially estimate accurate values of C_d.

5. Motion Computations for Regular Waves

The six degrees-of-freedom motions are computed by the present method for a finite depth for two typical semisubmersible rigs; MOHOLE and SEDCO 135-F. The computed motions for the SEDCO 135-F rig are compared with and validated by existing model test data [16], full-scale data [17], and the previous work [3] which computed all six degrees of motion. There are no model test data for the MOHOLE rig for a finite depth, and the validity is confirmed with the motions for infinite depth [4]. Another previous work [6] computed only heave, roll, and pitch motions of a different ("STAFLO") rig for a finite depth, used constant values of the added-mass coefficients and zero wave-damping coefficients, and made no comparison with any model test data. To the author's knowledge, there have been no more motion computations for the semisubmersible rigs in finite-depth water.

As previously described, usually wave components of periods, $T=5$ to 15 sec are of interest for the

drilling operations at sea, and wave components of $T>15$ sec are of great interest for the survival con ditions in the rough sea. Wave components of perhaps $T>25$ sec are very rarely encountered at sea. For a majority of the existing semisubmersible drilling rigs including the present two rigs, only the heave has its natural or resonance period below $T=25$ sec, and roll, pitch, surge, sway, and yaw all have their respective natural periods beyond $T=25$ sec.

Present Computation. The six degrees-of-freedom motions are computed for two semisubmersible drilling rigs of different configuration and arrangement of the rig members: MOHOLE and SEDCO 135-F. The MOHOLE drilling rig has a lateral symmetry and parallel hulls ($\gamma_i=0$), and additionally has a fore-and-aft symmetry for the present computations. So additional coefficients (7) and (8) in the coupled linear equations of motion (4) vanish; $A_{12}=A_{14}=A_{16}=A_{25}=A_{45}=A_{56}=A_{35}=0=B_{12}=B_{14}=B_{16}=B_{25}=B_{45}=B_{56}=B_{35}$, and $C_{34}=C_{35}=C_{45}=0$. The geometric characteristics of the MOHOLE rig used for the present computations are estimated from the rig drawing, and the other characteristics are directly from Bain [1] (see Table 3).

Table 3. Particulars of "MOHOLE" and "SEDCO 135-F" Rigs Used For the Motion Calculations

	MOHOLE	SEDCO 135-F (est.)
Displacement (L. tons)	22,813.0	17,657.0
(M. tons)	24,337.0	17,978.0
Draft (ft)	70.0 (21.34)*	80.0 (24.38)
VCG (ft)	67.5 (20.57)	64.7 (19.72)
Radii of gyration r_x (ft)	108.8 (33.16)	113.0 (34.44)
r_y (ft)	101.6 (30.97)	109.0 (33.22)
r_z (ft)	119.9 (36.55)	162.0 (49.38)
Column diameter (ft)	31.0 (9.14)	35.0 (10.67)
Hull diameter (ft)	35.0 (10.67)	— —
Effective hull length (ft)	340.0 (103.63)	100.0 (30.48)
Hull height (ft)	— —	25.0 (7.62)
Hull width (ft)	— —	60.0 (18.29)
Column spacing (ft)	130.0 (39.624)	280.0 (85.344)
Hull spacing (ft)	215.0 (65.532)	280.0 (85.344)
Approx. steel weight** (L. tons)	9,821.0	7,464.0
(M. tons)	10,000.0	7,600.0

*Numbers inside the parentheses are in metric unit.
**Exclude variable deck load.

The SEDCO 135-F. rig has a lateral symmetry; $A_{34}=0=B_{34}$ and $C_{34}=C_{45}=0$. The characteristics of the SEDCO 135-F rig are the same as those used for the model test [16] (see. Table 3): the footing geometry may not be represented by two-dimensional segments, and the coupling coefficients a_{jk} and b_{jk} (55), $j,k=1,2,3$ on the footing segments may not become zero, when $j\neq k$. Then the theory may not exactly apply to the footing. But the motion computations with the experimentally determined a_{jj} and b_{jj} only agree quite well with the model test data.

Since all the six equations of motion are strongly coupled, all six equations (4) are simultaneously solved with the coefficients (6), (7), and (8), and the exciting forces and moments (100). The numerical solution uses the matrix inversion technique.

As previously described, the present computations use the frequency dependent added mass and wave damping coefficients (Figs. 4 and 6). The added mass can significantly influence the heave natural period. The coefficients in Fig. 4 are computed by the Frank's method [5], include the free surface effect, and are used for the MOHOLE rig: as previously discussed in detail, there is little finite depth effect for the drilling draft used. The coefficients in Fig. 6 for the SEDCO 135-F rig includes both the free-surface and finite-depth effects and the hydrodynamic interference effect, since they are measured for an actual model. The viscous-damping coefficients used are $C_d=1.0$. C_d significantly affects the resonance motion which can be often nonlinear and can have the possible interference effects at the joints and between the rig members. So the viscous damping is empirically determined. The wave amplitude used for the computations is $A=15ft$ (4.572m).

Both the wave damping and the viscous damping (114) and (115) are both taken into account by b_{11} and b_{22} for the column segments and by b_{22} and b_{33} for the hull segments of the MOHOLE and additionally

by b_{11} for the SEDCO 135-F. As described above, the viscous damping components are expressed in terms of the viscous drag, C_d and the relative, oscillatory velocity, v_{ji}^r (118) and (119) for the column and hull segments. v_{ji}^r is also a function of the wave amplitude, A.

For the motion computations, initially C_d is selected from the wind-tunnel test data for a given geometry, and for the selected value of C_d the motions (displacements) are computed. For the motion computation, v_{ji}^r is initially unknown without computing the oscillatory velocity of the i^{th} segment or the motions of the floating rig. So initially the motion computations with the given C_d use $v_{ji}^r = \dot{x}_{ji} - \dot{x}_{ji}$ with $\dot{x}_{ji} = 0$: $\dot{x}_{ji}$ is the water-particle oscillatory velocity at the i^{th} point (x_{ci}, y_{ci}, z_i), and $\dot{x}_{ji}$ is the oscillatory velocity of the corresponding segment. Second time the initially computed motions, $\dot{x}_{ji}$, or the resulting, v_{ji}^r is used to compute the motions again. Then third time new v_{ji}^r is used to compute the motions. This iteration process for the given value of C_d continues until the computed motions converge to final values: except near the resonance frequency the computed motions converge fast. Then the final values of the computed motions are compared with the model test data. The damping, especially viscous damping significantly affects the motion near the resonance frequency. So the comparison of the motions for the given value of C_d can be made only for the modes of motion which have resonance frequency within the frequency range of interest. If the resonance amplitude of the computed motion is larger than the model test data, the value of C_d can be increased and the iteration repeats, and vice versa. A few more comparison studies in addition to the MOHOLE and SEDCO 135-F rigs are conducted. The result shows the value of C_d close to $C_d \approx 1.0$ uniformly for all the segments. Also for the drilling operational modes the viscous-damping effect on the motion near the resonance frequency is dominant over the wave damping.

Since the relative velocity v_{ji}^r is a function of A, the motion computations are affected through v_{ji}^r by the value of A which affects the amplitudes of both the water-particle oscillatory velocity, $\dot{x}_{ji}$ and the oscillatory motion velocity of the i^{th} segment, $\dot{x}_{ji}$. So the larger A is, the smaller the transfer function of the resonance motion, and vice versa.

Other Work. The previous work [3] used a direct extension to a floating structure of Morison's wave force equations [3] determined for a fixed pile structure: the present derivations indicate the limitations of the wave force equations of this kind. The motion calculations [3] use guessed constant-value added mass coefficients with no free-surface effect, consequently neglected wave damping coefficient, and empirically included viscous drag coefficients which require a guessing of rig's oscillation velocity for the damping force.

Experimental Data. The model test data [16] of motion amplitudes and phase angles for the SEDCO 135-F rig were obtained for the regular waves; the water depth was 120ft (36.58m), and the rig's drilling draft was 80ft (24.38m): the model had 9 mooring lines. The full-scale test data [17] of motion amplitudes (no phase angles analyzed) for the SEDCO 135-F rig were obtained off Vancouver coastline, British Columbia, Canada; the wave heading was not known, and water depths were between 180ft (54.9m) and 330 ft (100.6m). Due to the uncertainty in the accuracy of the full-scale data for modes of motions

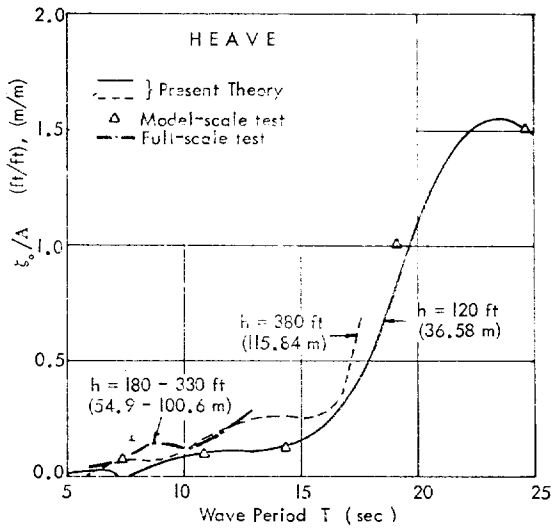

Fig. 7. Comparison of SEDCO 135-F Heave Predictions with Model-Scale and Full-scale Test Data.

other than heave, only the heave (Fig. 7) is used for the present motion correlation. For the MOHOLE rig, the model test data [10] are obtained for deep water: water depth is claimed to be infinite and the deep water case is already extensively treated [4]. The draft is 70 ft (21.34m).

Data Definition. In Figs. 7 to 14 the surge (ξ), sway (η), and heave (ζ), amplitudes in regular waves are presented as and referred to steady state response amplitude operators, or transfer functions (R_r); ξ_o/A, η_o/A, and ζ_o/A, respectively, and the roll (ϕ), pitch (θ), and yaw (Ψ) amplitudes as steady state transfer functions (R_r); ϕ_o/A, θ_o/A, and Ψ_o/A, respectively. These motion transfer functions are the steady state values, $(x_j)_o/A$ from the following expression,

$$\frac{x_j}{A}=\frac{(x_j)_o}{A}\cos(\omega t-\epsilon_j), \quad j=1,2,\ldots 6 \quad (122)$$

where ϵ_j are phase angles in degree as indicated in Figs. 7 to 14. The phase angles of motions are positive when the motions lag the wave, with the wave crest being at the rig CG as a reference.

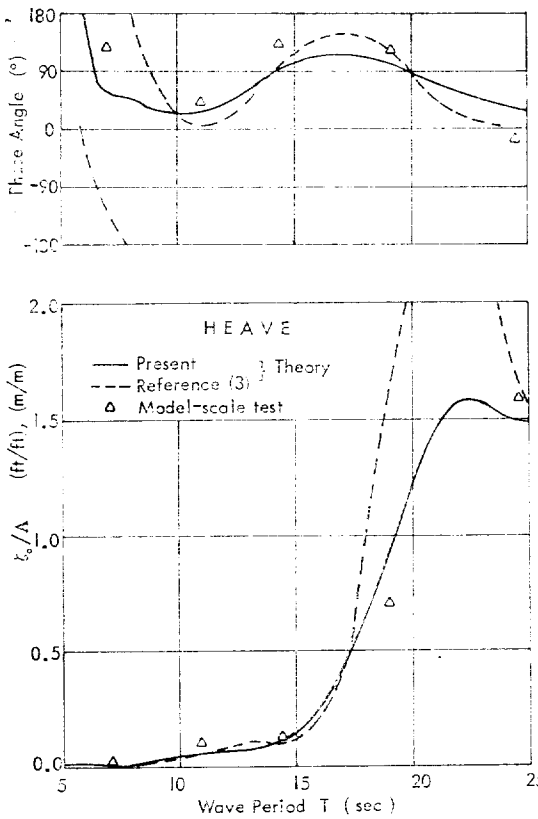

Fig. 8. Heave of SEDCO 135-F (waves 30° off bow; and h=120 ft (36.58m)).

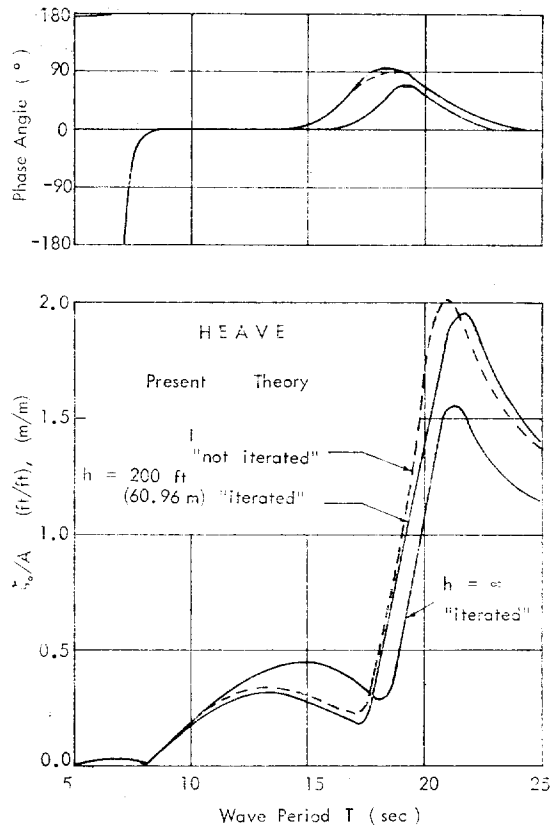

Fig. 9. Heave of MOHOLE (head waves; and h=200 ft (60.96m) and ∞).

5.1. Motion Comparisons

To test the present method's validity and accuracy in determining floating-rig motions in regular waves, motions predicted for the SEDCO 135-F rig in waves of finite (120 ft or 36.58m) water depth are compared with motions measured by model-scale tests [16] and full-scale heave tests [17]. Comparison shows good agreement Figs. 10 through 14 show good agreement between the present predictions and measured data for both amplitudes and phase angles of roll, pitch, surge, sway, and yaw motions. Finally, comparison of the present predicted motions (Figs. 8 to 14) with the previous work [3] shows that the present calculations are more accurate for both motion amplitudes and phase angles.

Heave Figure 7 shows for the SEDCO 135-F rig that the present heave prediction for the 120 ft

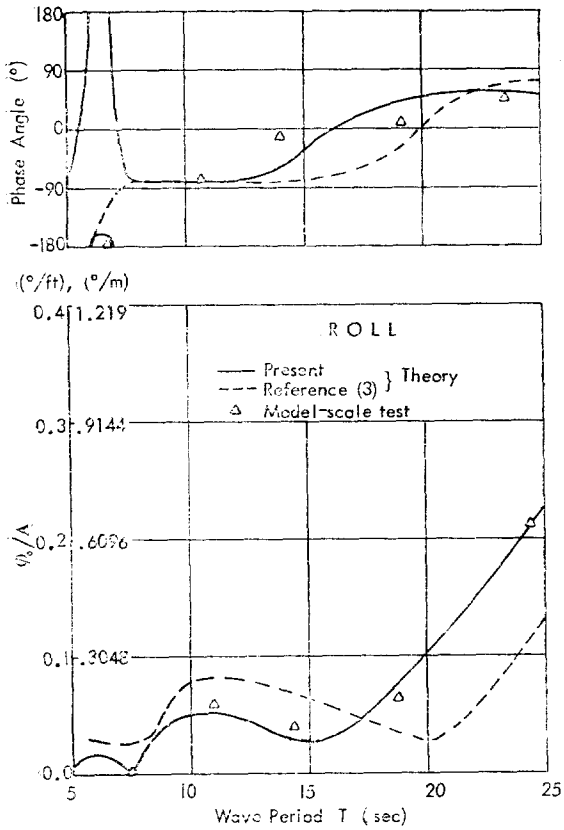

Fig. 10. Roll of SEDCO 135-F (beam waves; and h=120ft (36.58m)).

(36.58m) water depth agrees well over the wave period range with the model-scale test data obtained for the same condition. Another heave computation is made for the 380 ft (115.84m) water depth, since the full-scale data were measured for the various water depths. The full-scale heave data fall within the heave curves calculated for the two water depths. Note that Reference [17] does not show the full-scale data outside the wave period range indicated in Fig. 7. Figure 8 shows that the present heave calculation is more accurate for both amplitude and phase angle than the other computations [3]. Both the model-scale test data and the present computation show that the heave natural period is close to T=22 sec. The resonance heave motion may actually become nonlinear. The larger the damping forces, the smaller the heave amplitude near is resonance period. Sumerged member's surface of the full-scale rig is usually rougher due to marine fouling than that of the scaled model, and consequently viscous-damping force is expected to be larger for the full-scale rig; that is, the heave resonance amplitude is expected to be smaller than for the scaled model. The added-mass coefficients for the present heave calculation of the rig at the drilling draft are the experimental values (Fig. 6). Though not presented in this paper, comprehensive analysis [4] of the present method shows that a change of the wave direction relative to the rig heading does not significantly alter the heave amplitudes for the SEDCO 135-F rig, but significantly influences the heave phase angles. The wave period at which the minimum heave amplitude occurs depends on the column spacing and the distance between the hulls in beam waves, and the hull lengths or sizes in head waves.

Figure 9 shows the heave predictions for the MOHOLE rig for both infinite and finite depths: the finite depth is h=200 ft (60.96m). The infinite depth case [4] shows that the prediction agrees quite well with

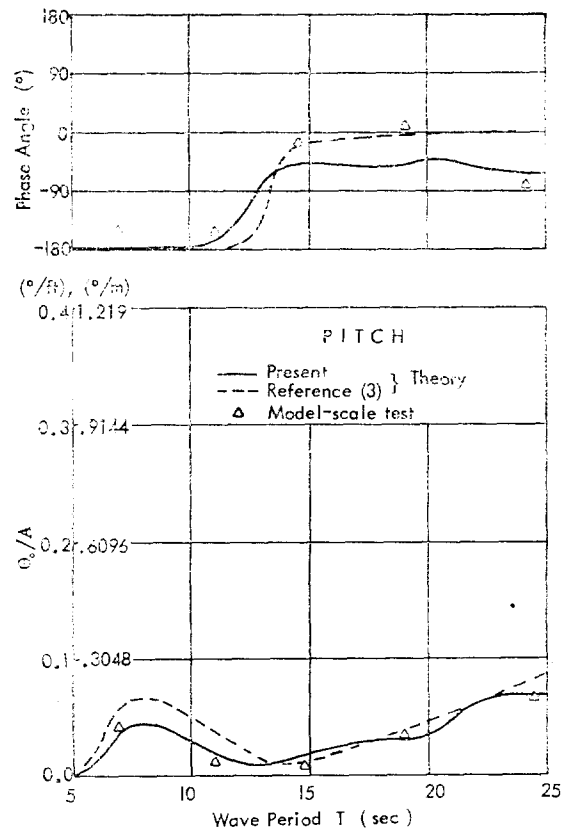

Fig. 11. Pitch of SEDCO-F (beam waves; and h=120 ft (36.58m)).

the model test data. Figures 7 and 10 show that the heave amplitudes are generally smaller up to $T \approx 18$ sec for the finite depth than for the infinite depth, and that the heave natural period is longer for the finite depth than for the infinite depth. Complete analysis of the water-depth effect on all six degrees-of-freedom motions has been underway. For the finite depth, two heave curves are shown: one is a final value after iteration of the relative oscillatory velocity and the other is the heave calculated with $v_j^r = \dot{x}_j$ which is the water-particle oscillatory velocity.

Other Modes of Motion. The present roll (Fig. 10) and pitch (Fig. 11) predictions for the SEDCO 135-F rig give good agreement in both the amplitudes and phase angles with the model-scale test data and clearly show better accuracy of roll predictions, as compared with the other's [3]. Notice that Fig. 10 shows non-zero pitch for beam waves. This is because this rig has three semi-submerged columns and submerged

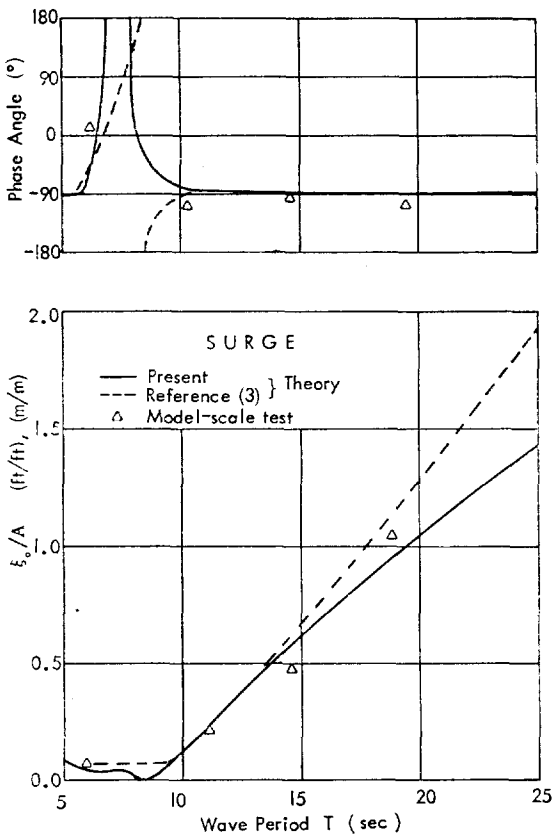

Fig. 12. Surge of SEDCO 135-F (waves 30° off bow; and h=120 ft (36.58m)).

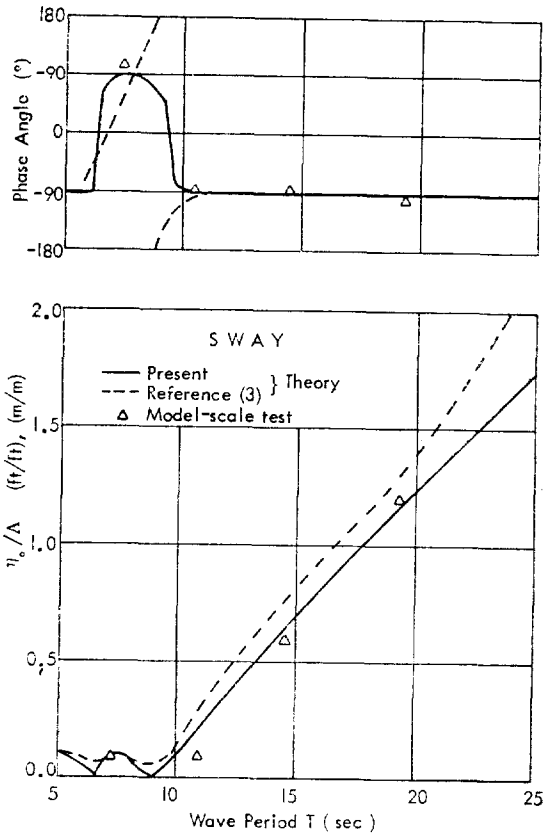

Fig. 13. Sway of SEDCO 135-F (beam waves; and h=120 ft (36.58m)).

footing hulls which are not symmetric about the y-axis when the incident waves act on the submerged portion of the rig members. On the other hand, many existing floating semisubmersible drilling rigs have symmetry about both the x- and y-axes, and amplitudes of the roll and pitch are zero for the head and beam waves, respectively.

Surge (Fig. 12) and sway (Fig. 13) predictions for the SEDCO 135-F rig agree well with the model-scale test data. Unlike ships' surge and sway, the surge in head waves and sway in beam waves are nearly the same on the order of magnitude of the amplitude for the present rig and most column-stabilized semisubmersible rigs.

Comparison of yaw motions in the present calculation and the scale-model test for the SEDCO 135-F rig gives good agreement in both the amplitude and phase angle (Fig. 14). This good agreement of yaw partly supports the assumption made above that the

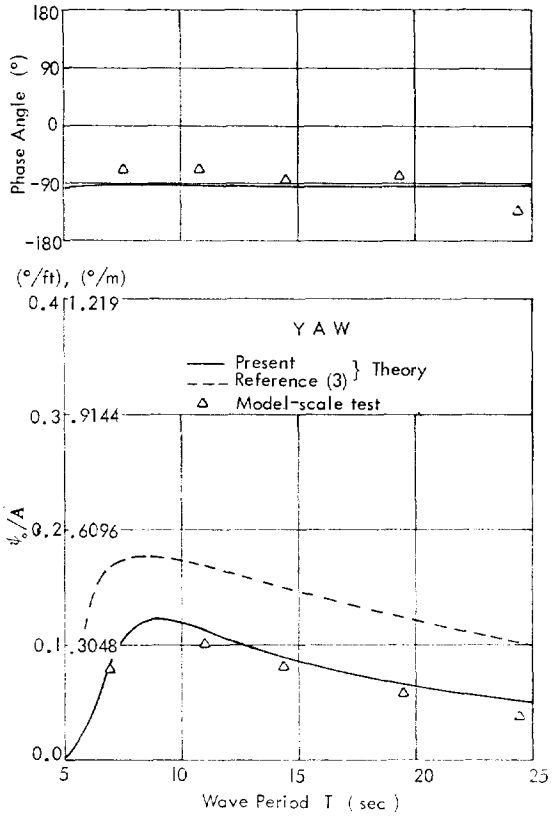

Fig. 14. Yaw of SEDCO 135-F (beam waves; and h=120 ft (36.58m)).

hydrodynamic end effect of the rig members can be neglected in the motion calculation. Fig. 14 also shows that the present prediction accuracy of yaw is better than the other's [3].

For the modes of motion other than heave which has its natural period within the wave period range of interest, the effects of the added mass and damping on motions are very small. This is because the added mass and damping forces significantly influence the motions only near the resonance periods and except for heave, the motion resonances occur at T>25 sec which has little practical significance. Coastal and ocean waves rarely possess wave components of T=25 sec. Therefore, for the modes of such floating structure's motion other than the heave, natural periods are longer than 25 seconds, and small errors in the added mass and damping coefficients in the equations of motion affect little of the accuracy of the calculated motions of those modes within the frequency range of interest.

6. Statistical Values of the Motion

The linear motions obtained for regular waves are used to predict response energy spectra and statistical values for motions in a given irregular sea, using spectral analysis. We can apply the proper wave spectrum for a specific seaway in a specified season to $R_r(\omega)$ to get motion energy spectra for the irregular sea. This statistical analysis does not give time history of the responses, but gives statistical description of the motions which can be used in preliminary design of a floating structure.

It is assumed that the irregular seaway and the response motions are random processes, that the random processes are represented by a stationary Gaussian distribution, and that the sum of the linear motions in response to a number of simple linear sinusoidal waves is equal to the motion responses to the sum of the waves-linear superposition principle. Under these assumptions, the rigs' motion response energy spectrum $R_s(\omega)$ can be represented by

$$R_s(\omega)=S_1(\omega)\ R_r^2(\omega) \tag{123}$$

where $S_1(\omega)$ is a wave specturum energy density and $R_r(\omega)$ is a motion transfer function such as given in Figs. 7 to 14.

Integration of $S_1(\omega)$ over the frequency gives wave energy E_1, and the integration of $R_s(\omega)$ over the frequency gives motion energy E_r. Based on the results of Longuet-Higgins [9], significant wave height (an averaged value of the 1/3-highest wave heights) and significant motion in double amplitude respectively can be obtained,

$$H_{1/3}=4.0\sqrt{E_1} \tag{124}$$

and

$$R_{1/3}=4.0\sqrt{E_r} \tag{125}$$

Using the Pierson-Moskowitz wave spectrum [13] for the $S_1(\omega)$, significant heaves ($\zeta_{1/3}$) in double amplitude are computed with two $R_r(\omega)$ of heave; the present computation and the other work [3] in Fig. 8. Figure 15 shows actual deviation of heaves between the two computations for the irregular waves.

For the present procedure of getting the statistical values of the motions, the inaccuracy in the motion

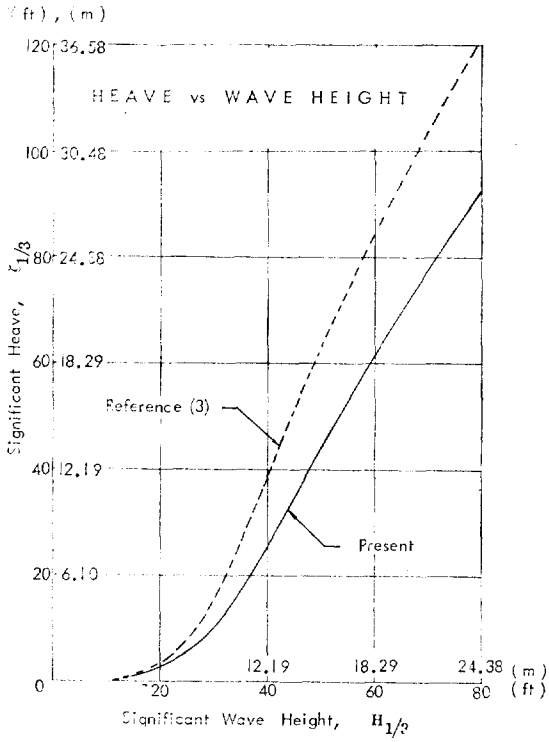

Fig. 15. Significant Heaves versus Significant Wave Heights (waves 30° off bow; and h=120 ft (36.58m)).

computation for the regular waves can result in significant error or deviation (Fig. 15) in the statistical values of the motion. Usually this statistical analysis of motions for the irregular waves has been a simple method in design. Nonlinearity problem exists for high sea state and is not discussed here, since it is beyond the scope of the present paper.

Table. 4. Useful Statistical Values

Wave Height Relationship [9]	Response Relationship
$H_{avg}/H_{1/3}$ 0.626	$R_{avg}/R_{1/3}$ 0.626
$H_{1/10}/H_{1/3}$ 1.271	$R_{1/10}/R_{1/3}$ 1.271
$H_{1/100}/H_{1/3}$ 1.672	$R_{1/100}/R_{1/3}$ 1.672
$H_{max}/H_{1/3}$ 1.77	$R_{max}/R_{1/3}$ 1.77

Average wave period [13]:

$$T_{avg}=1.96\sqrt{H_{1/3}}$$

Pericd at which the maximum value of $S_1(\omega)$ occurs [13]:

$$T_{max}=2.76\sqrt{H_{1/3}}$$

Average apparent wavelength [13]:

$$\lambda_{avg}\approx 13.14\sqrt{H_{1/3}}$$

The probability of occurance that the response $R_{1/3}$ exceeds a prespecified response $\bar{R}_1$ for a large number N of $R_{1/3}$ values is

$$P\{R>\bar{R}_1\}=\exp\left[-\bar{R}_1^2/R_{1/3}^2\right] \quad (126)$$

and the most probable largest response value is

$$\bar{R}_N=0.707\ R_{1/3}\ (ln\ N)^{1/2} \quad (127)$$

Selection of N is described in [9]. As practical reference, other useful statistical values listed in Table 4.

References

1. Bain, J.A.: "Extension of MOHOLE Platform Force and Motion Studies," *Project MOHOLE Report by General Electric Co.* (October, 1964).
2. Blagoveshchensky, S.N.; *Theory of Ship Motion*, Dover (1962).
3. Burke, B.G.;" The Analysis of Motions of Semi-submersible Drilling Vessels in Waves," *Proc. Offshore Tech. Conf., Houston, Texas* (April 19 69), *Paper* No. 1024.
4. Chung, J.S.; "Motions of Semisubmersible Drilling Rigs in Deep Water," *J. of the Society of Naval Architects of Korea*, Vol.11, No.2 (1974).
5. Frank, W.; "Oscillation of Cylinder in or Below the Free Surface of Deep Fluids," *Naval Ship R & D Center Report* 2357 (1967).
6. Hooft, J.P.; "A Mathematical Method of Determining Hydrodynamically Induced Forces on a Semi-Submersible," *Trans. SNAME* (1971).
7. Ippen, A.T.; *Estuary and Coastline Hydrodynamics*, McGr-awHill (1966).
8. Kim, C.H., and Chou, F.; "Motions of a Semi-Submersible Drilling Platform in Head Seas," *Davidson Laboratory Report*, OE 71-8 (Dec. 1971).
9. Longuet-Higgins, M.S.; "On the Statistical Distribution of the Heights of Sea Waves." *J. of Marine Research*, Vol.2, No.3 (1952), pp. 245-265.
10. McClure, A.C.; "Development of the Project MOHOLE Drilling Platform," *Trans. SNAME* (1965), p. 50-99.
11. Ochi, M.K. and Vuolo, R.M.; "Seakeeping Characteristics of a Multi-Unit Ocean Platform," *Trans. SNAME* (1971).
12. Paulling, J.R.; "Elastic Response of Stable Plat-

form Structures to Wave Loading," *Int'l Symp. on the Dynamics of Marine Vehicles and Structures in Waves, Inst. of Mech. Eng'rs*, London (April 1-5, 1974), pp. 263-272.

13. Pierson, W.J.; and Moskowitz, L., "A Proposed Spectral Form for Fully Developed Wind Seas Based on the Similarity Theory of S.A. Kitaigorodskii," *J. of Geophysical Research*, Vol.69, No.24 (Dec. 15, 1964).
14. Salveson, N., Tuck, E.O., and Faltinson, O.; "Ship Motions and Loads," Trans. *SNAME* (1970), pp. 250-287.
15. St. Dennis, M.; "On the Motions of Oceanic Platforms," *Int'l Symp. on the Dynamics of Marine Vehicles in Waves, Inst. of Mech. Eng'rs* London (April 1-5, 1974), pp. 121-142.
16. Van de Voorde, C.B., and Lap, A.J.W.; "Model Tests for the SEDCO-Floating Drilling Platform" (unpublished).
17. Watts, J.S., et al.; "A Performance Review of the SEDCO 135-F Semisubmersible Drilling Vessel," *Proc. Petroleum Society of CIM*, Calgary, CANADA (May, 1968).
18. Mercier, J.A.; "Hydrodynamic Forces on Some Float Forms, *J. of. Hydronautics*, Vol.5, No. 4 (Oct. 1971), pp. 109-117.
19. Wendel, K.; "Hydrodynamic Mass and Hydrodynamic Moments of Inertia," *DTMB Translation* 260 (1956).
20. Wiegel, R.L.; *Oceanographical Engineering*, Prentice-Hall, 1964. pp. 254.
21. Sao, K., Maeda, H., and Hwang, J.H.; "On the Heaving Oscillation of a Circular Dock," *J. of Zosen Kyokai*, Vol. 130(1971), pp. 121-130.